

Contents

1	Introduction	1
1.1	General Motivation for Electrolyte Modeling	1
1.2	Literature Review	1
2	Electrolyte Model	3
2.1	Basic Quantities	3
2.2	Closure of the system	5
2.3	Assumptions	5
2.4	Comparison to Nernst-Planck Model	6
2.5	Solvation Effect	6
2.6	The Incompressible Limit	7
2.7	Ternary Electrolyte	7
2.8	Dimensionless Quantities	7
3	One-Dimensional Equilibrium	9
3.1	Incompressible Limit	9
3.2	Neglecting the Pressure Dependency	10
3.3	The Charge of the System	10
4	Numerical Implementation	12
4.1	Variational Formulation	12
4.2	Numerical Treatment of Nonlinearity	13
4.3	Validation	13
4.4	Convergence	14
5	Results	16
5.1	Ternary Electrolyte	16
5.2	One-Dimensional Equilibrium - An Instructive Example	17
5.3	Analysis of Parameter	20
5.3.1	Electric Potential and Pressure	21
5.3.2	Atomic Fractions	22
5.4	Comparison to classical Nernst-Planck model	23
5.5	Solvation Effect	24
5.6	Compressibility	26
5.7	Double Layer Capacity	28
5.7.1	Influence of Molarity	29
5.7.2	Influence of Dimensionless Parameter λ^2	29
5.7.3	Influence of Compressibility	30
5.8	Many Constituent Mixture	30
5.8.1	Four Constituents	31
5.8.2	Five Constituents	32
5.8.3	Six Constituents	33
5.8.4	Electric Potential in a Many Constituent Mixture	33

5.9	2D-Results	33
5.9.1	Electric Diode	33

List of Figures

1.1	Dimensionless calculations. The atomic fractions are not limited to the interval $[0,1]$ in the Nernst-Planck model.	2
1.2	Dimensionless calculations. The DGM model prevents the atomic fractions to leave the range of $[0,1]$	2
4.1	Placeholder -> Update with *.svg, analyze while x-scaling wrong, write texts	14
4.2	Convergence	15
5.1	Ternary electrolyte	17
5.2	Solutions for different L_x with $\lambda^2 = 1 \cdot 10^{-3}$, $z_A = -1$, $z_C = 1$	19
5.3	Streamplot of the solution at the left-most point for the electric potential	20
5.4	Influence of the potential difference and the dimensionless parameter λ on the electric potential and the pressure	21
5.5	Scaling of the electric potential	22
5.6	Influence of the potential difference and the dimensionless parameter λ on the atomic fractions	23
5.7	Value of the atomic fractions at the left boundary for different applied voltage differences	24
5.8	Influence of a on the pressure	25
5.9	Comparison DGM model to Poisson-Boltzmann model	26
5.10	Convergence from DGM model towards Poisson-Boltzmann model	27
5.11	Effect of Solvation	27
5.12	Compressibility	28
5.13	Calculation of the charge stored in the boundary and the double layer capacity for different molarities	29
5.14	Calculation of the charge stored in the boundary and the double layer capacity for different values of λ^2	30
5.15	Calculation of the charge stored in the boundary and the double layer capacity for different compressibilities	30
5.16	Atomic fractions (left axis) and pressure (right axis) for all four different mixtures	31
5.17	Electric Potential for all four different mixtures	32
5.18	Forward Bias (top, $\varphi_{\text{bias}} = 10$), no bias (center, $\varphi_{\text{bias}} = 0$) and backward bias (bottom, $\varphi_{\text{bias}} = -10$)	35

List of Symbols

Constants

Variable	Value & Unit	Property
ϵ_0	$1.602 \cdot 10^{-19} [\text{As}]$	Dielectric constant
e_0	$8.85 \cdot 10^{-12} [\text{F}]$	Elementary charge
k	$1.381 \cdot 10^{23} [\text{J/K}]$	Boltzmann constant
N_A	$6.022 \cdot 10^{23} [1/\text{mol}]$	Avogadro constant

Species Properties

Variable	Unit	Property
n_α	$[1/\text{m}^3]$	Number density
y_α	$[-]$	Atomic fraction
m_α	$[\text{kg}]$	Atomic mass
z_α	$[-]$	Charge number
\mathbf{J}_α	$[\text{kg}/\text{m}^2\text{s}]$	Diffusion flux
g_α	$[\text{J}/\text{kg}]$	Specific Gibbs energy
g_α^{ref}	$[\text{J}/\text{kg}]$	Reference specific Gibbs energy
μ_α	$[\text{J}/\text{kg}]$	Chemical potential
κ_α	$[-]$	Solvation number
v_α	$[\text{m}/\text{s}]$	Velocity
u_α	$[\text{m}/\text{s}]$	Diffusion velocity
ρ_α	$[\text{kg}/\text{m}^3]$	Partial mass density

Mixture Properties

Variable	Unit	Property
φ	$[\text{V}]$	Electric potential
p	$[\text{Pa}]$	Pressure
n	$[1/\text{m}^3]$	Total number density
T	$[\text{K}]$	Temperature
K	$[\text{Pa}]$	Bulk modulus
n^{ref}	$[1/\text{m}^3]$	Reference number density

n^F	$[1/\text{m}^3]$	Space charge
χ	$[-]$	Dielectric susceptibility
$\mathbf{M}_{\alpha\beta}$	$[\text{kgKs}/\text{m}^3]$	Kinetic matrix
\mathbf{v}	$[\text{m}/\text{s}]$	Barycentric velocity
ρ	$[\text{kg}/\text{m}^3]$	Total mass density

Indexing

Variable	Meaning
\cdot^{ref}	Reference state of \cdot
\cdot^L	Value of property \cdot at left boundary
\cdot^R	Value of property \cdot at right boundary
$\delta\cdot = \cdot^L - \cdot^R$	Difference from left to right boundary for property \cdot
\cdot_α	Property \cdot of species α

Abstract

Chapter 1

Introduction

1.1 General Motivation for Electrolyte Modeling

More and more devices are powered with electrical energy, such as smartphones, laptops, bicycles and cars. Therefore, the need to produce and store electricity efficiently is increasing rapidly and batteries, as a portable energy source, are becoming a key technology of the future. Not only the usage of portable energy but also renewable energies, are getting more and more important in the future. Those renewable energies are key to reducing greenhouse gas releases. However, the balance between the production and consumption of energy is crucial. The production time of alternative energy resources, such as solar and wind energy, cannot be determined, leading to a high need for efficient energy storage, such as batteries, to enable renewable energies. Batteries consist of three major components, namely the cathode, anode and the electrolyte. The cathode and anode are positive and negative electrodes, consisting of a porous material to increase the effective surface area and capacity of each electrode. In a standard lithium-ion battery, lithium ions create an electrical potential between the anode and cathode terminals. The electrolyte is used as a “separator” between the cathode and anode and allows the lithium-ions to pass through while blocking other electrons. In the charging process, lithium-ions move through the electrolyte from the positive side to the negative side. In the discharging process, the lithium-ions move in the other direction. The movement of the ions creates an electrical potential difference which then can be used to power an electrical device.

Due to the increased need for battery storage, it is important to optimize batteries further. Lifetime, charging time and energy loss are just a few aspects, which need further optimization to prepare for a greener future. There are several ways how to design better-performing batteries in the future. Numerical simulations are important for understanding the drawbacks of batteries to then create new optimized batteries. Such simulations can also be used to try out new battery configurations. For example, there are billions of possible combinations of components that can be interchanged. Simulations can do this efficiently in just a few seconds or minutes, while it is costly and very time-consuming to build all different combinations in “real” batteries to test them.

To sum it up, batteries are a key technology for a decarbonized future. However, further optimized batteries are very important to enable renewable energy resources and to reduce the release of greenhouse gases. Numerical simulations are a key aspect of creating better-performing, longer-lasting and faster-charging batteries of the future.

1.2 Literature Review

There are several models for describing the complex behavior of electrolytes. One of the oldest, but still widely used models is the classical Nernst-Planck model (see [16, 17, 15]). This model relies on the assumption of dilute solutions and neglects the ion-solvent interaction. Therefore, the model has no mechanism to limit the amount of the number densities in the boundary layer and fails to predict their correct distribution (compare with Figure 1.1). The model misses, that there are only $N - 1$ independent diffusion fluxes (compare with [3]).

In 2006 Tomáš Roubíček proposed a model, combining Navier-Stokes equations for barycentric velocities with Nernst-Planck's equations for concentrations, the heat equation and the Poisson equation for a quasi-static electric field (compare with [19]). Roubíček's paper introduces the correct coupling of the $N - 1$ diffusion fluxes but violates the 2nd Law of Thermodynamics (see [3]).

A. Prohl and M. Schmuck inspected the incompressible Navier-Stokes-Nernst-Planck-Poisson system in 2010 (see [18]). They introduced two different schemes for solving the system of equations.

In this work, the Electrolyte model proposed by Dreyer, Gohlke and Müller in 2013 (see [3]), which is also referred to as the DGM model, is investigated. This system is based on a consistent application of principles of non-equilibrium thermodynamics, includes ion volume and solvation effects and consistently couples transport equations to momentum balance (compare with [8]). This coupling enables the model to predict physically meaningful values at the electrolyte boundaries, preventing the atomic fractions from exceeding the interval $[0, 1]$ (compare with Figure 1.2). This new model was further inspected by Dreyer, Gohlke and Landstorfer in 2013 (see [2]) and by Dreyer, Gohlke and Müller in 2014 (see [4]).

The DGM model has already been investigated by different researchers. In 2015, Braun, Yada and Latz (see [1]) investigated the DGM model in a stationary, one-dimensional setting and derived a semi-analytical solution to this. Furthermore, they inspected the influence of different parameters on the space charge layer formation. Jürgen Fuhrmann reformulated the DGM model in 2015 (see [9]) and 2016 (see [6]) using absolute activities as basic variables. Fuhrmann utilized a finite volume scheme to derive a numerical solution for the DGM model. In 2018 (see [8]) and in 2021 (see ([10])) Fuhrmann further investigated the DGM model.

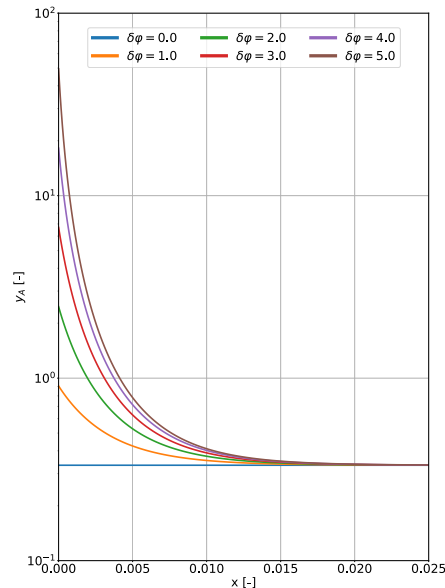


Figure 1.1: Dimensionless calculations. The atomic fractions are not limited to the interval $[0, 1]$ in the Nernst-Planck model.

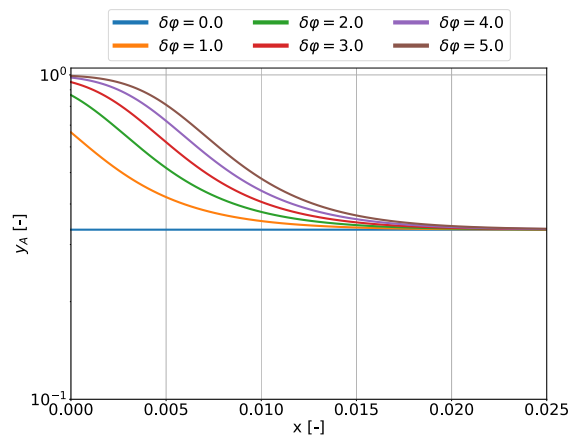


Figure 1.2: Dimensionless calculations. The DGM model prevents the atomic fractions to leave the range of $[0, 1]$

Chapter 2

Electrolyte Model

Consider a three dimensional spatial domain $\Omega \in \mathbb{R}^3$, which is occupied by a liquid mixture of N different constituents (also called species or components). Each constituent has its own density (ρ_α) and velocity (\mathbf{v}_α), where index \cdot_α denotes property \cdot of constituent α . The mixture has a temperature (T) and a local electric field (E). Each of these properties is a scalar and changes in space and time.

$$[n_\alpha, v_\alpha, T, E] : \Omega \times \mathbb{R}^+ \rightarrow \mathbb{R} \quad \alpha \in \{1, \dots, N\} \quad (2.1)$$

2.1 Basic Quantities

The partial mass densities are given by

$$\rho_\alpha = m_\alpha n_\alpha \quad (2.2)$$

with the atomic mass m_α and the number density n_α and the total mass density is defined as the sum over all partial mass densities

$$\rho = \sum_{\alpha=1}^N \rho_\alpha \quad (2.3)$$

The total number density of the mixture is represented by n and the atomic fractions of each constituent by y_α .

$$n = \sum_{\alpha=1}^N n_\alpha \quad (2.4)$$

$$y_\alpha = \frac{n_\alpha}{n} \quad (2.5)$$

$$\sum_{\alpha=1}^N y_\alpha = 1 \quad (2.6)$$

The atomic fractions are bounded to be between the lower limit of zero and the upper limit of one ($0 \leq y_\alpha \leq 1$).

The velocity of the mixture \mathbf{v} is defined as

$$\mathbf{v} = \frac{1}{\rho} \sum_{\alpha=1}^n \rho_\alpha \mathbf{v}_\alpha \quad (2.7)$$

with partial velocity \mathbf{v}_α .

The mass flux is given b

$$\mathbf{J}_\alpha = \rho_\alpha \mathbf{u}_\alpha \quad (2.8)$$

with the diffusion velocity \mathbf{u}_α .

$$\mathbf{u}_\alpha = \mathbf{v}_\alpha - \mathbf{v} \quad (2.9)$$

From these definitions the sum over all mass fluxes concludes as

$$\sum_{\alpha=1}^N \mathbf{J}_\alpha = 0 \quad (2.10)$$

Furthermore, the space charge is represented by

$$n^F = \sum_{\alpha=1}^N z_\alpha e_0 n_\alpha \quad (2.11)$$

Balance Equations for Mass, Momentum and Poisson Equation

With the definition of the diffusion velocity and diffusion flux, the partial mass balance can be identified as

$$\partial_t \rho_\alpha + \operatorname{div}(\rho_\alpha \mathbf{v}_\alpha) = \tau_\alpha \quad (2.12)$$

$$\Leftrightarrow \partial_t \rho_\alpha + \operatorname{div}(\rho_\alpha \mathbf{v} + \mathbf{J}_\alpha) = \tau_\alpha \quad \alpha \in \{1, \dots, N\} \quad (2.13)$$

Summing up the partial mass balances, the total mass balance follows ($\sum_{\alpha=1}^{N-1} \tau_\alpha = 0$)

$$\partial_t \rho + \operatorname{div}(\rho \mathbf{v}) = 0 \quad (2.14)$$

The total momentum balance reads

$$\partial_t(\rho \mathbf{v}) + \operatorname{div}(\rho \mathbf{v} \otimes \mathbf{v} - \boldsymbol{\sigma}) = \rho \mathbf{b} + \mathbf{k} \quad (2.15)$$

and is derived by summing up all partial momentum balances. $\boldsymbol{\sigma}$ is the stress tensor, $\rho \mathbf{b}$ some force density due to gravitation and inertia with the assumption $\mathbf{b} = 0$ (compare with [3]) Without magnetic contributions, the Lorentz force follows as

$$\mathbf{k} = n^e \mathbf{E} \quad (2.16)$$

with Maxwell's equations for quasi-static electric fields

$$\epsilon_0 \operatorname{div}(\mathbf{E}) = n^e \quad (2.17)$$

$$\mathbf{E} = -\nabla \varphi \quad (2.18)$$

where ϵ_0 is the dielectric constant and φ the electric potential. The electric field \mathbf{k} can be rewritten as

$$\mathbf{k} = \epsilon_0 \operatorname{div}(\mathbf{E}) \mathbf{E} = \operatorname{div} \left(\epsilon_0 (\mathbf{E} \otimes \mathbf{E} - \frac{1}{2} |\mathbf{E}|^2) \right) \mathbf{1} \quad (2.19)$$

$\mathbf{1}$ denotes the unit matrix.

Putting all this together, the momentum conservation is represented by

$$\partial_t(\rho \mathbf{v}) + \operatorname{div}(\rho \mathbf{v} \otimes \mathbf{v}) + \nabla p = -n^F \nabla \varphi \quad (2.20)$$

with the pressure p . The electric potential is described by a Poisson equation

$$-\epsilon_0(1 + \chi) \Delta \varphi = n^F \quad (2.21)$$

where χ is the dielectric susceptibility of the mixture and Δ the Laplace operator ($\Delta f = \operatorname{div}(\operatorname{grad} f)$).

Full System of Equations

The full system of equations is given by the first $N-1$ partial mass balances, the total mass and momentum balance and the Poisson equation for the electric potential

$$\partial_t(m_\alpha n_\alpha) + \text{div}(m_\alpha n_\alpha \mathbf{v} + \mathbf{J}_\alpha) = 0 \quad \alpha \in \{1, \dots, N-1\} \quad (2.22)$$

$$\partial_t \rho + \text{div}(\rho \mathbf{v}) = 0 \quad (2.23)$$

$$\partial(\rho \mathbf{v}) + \text{div}(\rho \mathbf{v} \otimes \mathbf{v}) + \nabla p = -n^F \nabla \varphi \quad (2.24)$$

$$-\epsilon_0(1 + \chi)\Delta \varphi = n^F \quad (2.25)$$

Due to the relation that all diffusion fluxes sum up to zero and all partial number densities sum up to the total number density, only the first $N-1$ partial mass balances are taken into account. This system of partial differential equations can be solved to get the density, velocity and electric potential of the mixture and the partial number densities for each species. It remains to find a closure for the diffusion fluxes and the pressure.

2.2 Closure of the system

The $N-1$ diffusion fluxes are calculate with

$$\mathbf{J}_\alpha = - \sum_{\beta=1}^{N-1} \mathbf{M}_{\alpha\beta} \left(\nabla \frac{\mu_\beta - \mu_N}{T} + \frac{1}{T} \left(\frac{z_\beta}{m_\beta} - \frac{z_N}{m_N} \right) \nabla \varphi \right) \quad \alpha \in \{1, \dots, N-1\} \quad (2.26)$$

with the positive defined kinetic matrix $\mathbf{M}_{\alpha\beta}$, the chemical potentials μ_α , the temperature T and the charge numbers z_α . The chemical potentials, μ_α , are given by

$$\mu_\alpha = g_\alpha + \frac{kT}{m_\alpha} \ln \left(\frac{n_\alpha}{n} \right) \quad (2.27)$$

where k represents the Boltzmann constant and g_α the specific Gibbs energy

$$g_\alpha = g_\alpha^R + \frac{K}{m_\alpha n^{\text{ref}}} \ln \left(\frac{n}{n^{\text{ref}}} \right) \quad (2.28)$$

with the reference number density n^{ref} , the reference chemical potential g_α^{ref} and the Bulk modulus K . The closure for the elastic pressure p is given by

$$p = p^{\text{ref}} + K \left(\frac{n}{n^{\text{ref}}} - 1 \right) \quad (2.29)$$

2.3 Assumptions

Throughout this work, the system is assumed to be in hydrostatic or mechanical equilibrium. Therefore, $\mathbf{v} = 0$ can be assumed, without loss of generality (compare with [6]). Furthermore, only the stationary case is considered, which leads to vanishing time derivatives. The kinetic matrix $\mathbf{M}_{\alpha\beta}$ is assumed to be diagonal and the system is isothermal; the temperature will be denoted as T_0 from now on, chemical reactions are permitted and gravity is ignored (see [3]). Furthermore, the neutral solvent (index N) is considered to be electroneutral, $z_N = 0$.

With these assumptions, the total mass balance from the system of equations 2.22-2.25 can be dropped and the partial mass balances and the total momentum balance simplify. The remaining system of equations is

$$\text{div}(\mathbf{J}_\alpha) = 0 \quad \alpha \in \{1, \dots, N-1\} \quad (2.30)$$

$$\nabla p = -n^F \nabla \varphi \quad (2.31)$$

$$-\epsilon_0(1 + \chi)\Delta \varphi = n^F \quad (2.32)$$

In the regions where the space charge, n^F is nonzero, the electric potential φ becomes a driving force for the calculation of the pressure, as it is described in the simplified momentum equation 2.31). The Poisson equation 2.32 describes the electric potential φ in the electrolyte under consideration of the space charge. The diffusion fluxes \mathbf{J}_α can be calculated with

$$\mathbf{J}_\alpha = -M_{\alpha\beta} \left(\nabla \frac{\mu_\beta - \mu_N}{T_0} + \frac{1}{T_0} \left(\frac{z_\beta}{m_\beta} - \frac{z_N}{m_N} \right) \nabla \varphi \right) \quad \alpha \in \{1, \dots, N-1\} \quad (2.33)$$

Note that the temperature T_0 in the first term is in the derivative, while it is in front of the derivative in the second term. However, this is of less importance, since the system is assumed to be isothermal. Additionally, 2.29 is reformulated to n and plugged into 2.28

$$n = n^{\text{ref}} \left(1 + \frac{p - p^{\text{ref}}}{K} \right) \quad (2.34)$$

$$g_\alpha = g_\alpha^{\text{ref}} + \frac{K}{m_\alpha n^{\text{ref}}} \ln \left(1 + \frac{p - p^{\text{ref}}}{K} \right) \quad (2.35)$$

The variables of interest are the electric potential, the total number density and the number densities of each species. However, it is convenient to calculate the atomic fractions for each species instead of the number density. The variables of interest change from (φ, n_α, n) to (φ, y_α, n) for $\alpha \in \{1, \dots, N-1\}$.

Recalling, that the atomic fractions sum up to one, the fraction for the neutral solvent can be calculated as

$$y_N = 1 - \sum_{\alpha=1}^{N-1} y_\alpha \quad (2.36)$$

2.4 Comparison to Nernst-Planck Model

The newly proposed diffusion flux combines the gradients of the chemical potentials of constituent α , the gradient of the chemical potential of the neutral solvent and the gradient of the electric potential. Comparing this to the classical Nernst-Planck flux

$$\mathbf{J}_\alpha = -M_\alpha^{\text{NP}} \left(k \nabla n_\alpha + z_\alpha e_0 n_\alpha \nabla \varphi \right) \quad \alpha \in \{1, \dots, N\} \quad (2.37)$$

with the Nernst-Planck mobility's $M_\alpha^{\text{NP}} > 0$. The Nernst-Planck model does not take into account that there are only $N-1$ independent diffusion fluxes. Next, it ignores the gradient of the chemical potential of the neutral solvent. This leads to a nonphysical behavior in the boundary layers for the classical Nernst-Planck diffusion flux.

2.5 Solvation Effect

Solvation leads to a rise of microscopic electrostatic interactions between the solvent and the ionic species, given by microscopic dipoles of solvent molecules (compare with [5]). This leads to a clustering of finite numbers of solvent molecules around an ion.

The solvation number κ_α describes the different scales of solvation. The larger the number, the more solvent molecules assemble around an ion. The neutral solvent has no solvation number, by definition, leading to $\kappa_N = 0$. In this work, a constant solvation number for all charged constituents, $\kappa_\alpha = \kappa$, is assumed. Since solvation leads to a clustering around ions, this effect can be modeled with the rather simple approximation $v_\alpha^{\text{ref}} = (\kappa + 1)v_N^{\text{ref}}$, with v_α^{ref} the specific volume of constituent α (compare with [5]).

Integrating this simple approximation into the representation of the electrolyte model, the definition of the specific Gibbs energy changes to:

$$g_\alpha = g_\alpha^{\text{ref}} + (\kappa + 1) \frac{K}{m_\alpha n^{\text{ref}}} \ln \left(1 + \frac{p - p^{\text{ref}}}{K} \right) \quad (2.38)$$

$$g_N = g_N^{\text{ref}} + \frac{K}{m_\alpha n^{\text{ref}}} \ln \left(1 + \frac{p - p^{\text{ref}}}{K} \right) \quad (2.39)$$

2.6 The Incompressible Limit

An incompressible mixture is assumed to fulfill $K \rightarrow \infty$. Plugging this limit in equation 2.38 leads to

$$\lim_{K \rightarrow \infty} g_\alpha = \lim_{K \rightarrow \infty} \left(g_\alpha^{\text{ref}} + (\kappa + 1) \frac{K}{m_\alpha n^{\text{ref}}} \ln \left(1 + \frac{p - p^{\text{ref}}}{K} \right) \right) \quad (2.40)$$

$$= g_\alpha^{\text{ref}} + (\kappa + 1) \frac{K}{m_\alpha n^{\text{ref}}} (p - p^{\text{ref}}) \quad (2.41)$$

For a detailed proof see Appendix 5.9.1.

Incompressibility leads to a constant total number density n .

$$n = n^{\text{ref}} \quad (2.42)$$

2.7 Ternary Electrolyte

A ternary electrolyte consists of three constituents ($N = 3$). Namely the negative charged anions ($A, \alpha = 1$), positive charged cations ($C, \alpha = 2$) and the neutral solvent ($S, \alpha = 3$). The space charge for a ternary electrolyte reads

$$n_{\text{ternary}}^F = \sum_{\alpha=1}^2 z_\alpha e_0 n_\alpha = e_o (z_A n_A + z_C n_C) \quad (2.43)$$

2.8 Dimensionless Quantities

In the following, some dimensionless quantities are introduced to scale the physical values to some reference level. The dimensionless quantities are defined as follows[3].

$$\begin{aligned} n &\rightarrow n^{\text{ref}} n, & p &\rightarrow p^{\text{ref}} p, & L &\rightarrow L^{\text{ref}} L, & z_\alpha &\rightarrow e_0 z_\alpha, & K &\rightarrow p^{\text{ref}} K \\ n^F &\rightarrow n^R e_0 n^F, & g_\alpha &\rightarrow \frac{kT_0}{m_\alpha} g_\alpha, & \mu_\alpha &\rightarrow \frac{kT_0}{m_\alpha} \mu_\alpha, & \varphi &\rightarrow \frac{kT_0}{e_0} \varphi \\ x &\rightarrow Lx \end{aligned}$$

Inserting the dimensionless quantities in the equations 2.30-2.35, with solvation effects, yields

$$\lambda^2 \Delta \varphi = -L^2 n^F \quad (2.44)$$

$$a^2 \nabla p = -n^F \nabla \varphi \quad (2.45)$$

$$\text{div}(\mathbf{J}_\alpha) = 0 \quad \alpha \in \{1, \dots, N-1\} \quad (2.46)$$

with the dimensionless flux

$$\mathbf{J}_\alpha = \nabla (\mu_\alpha - \mu_N + z_\alpha \varphi) \quad (2.47)$$

and

$$\mu_\alpha = g_\alpha + \ln(y_\alpha) \quad (2.48)$$

$$g_\alpha = g_\alpha^{\text{ref}} + (\kappa + 1)a^2(p - 1) \quad (2.49)$$

$$\lambda^2 = \frac{kT_0\epsilon_0(1 + \chi)}{e_0^2 n^{\text{ref}} (L^{\text{ref}})^2} \quad (2.50)$$

$$a^2 = \frac{p^{\text{ref}}}{n^{\text{ref}} K T_0} \quad (2.51)$$

$$L = 1 \quad (2.52)$$

$$n^F = n \sum_{\alpha=1}^{N-1} z_\alpha y_\alpha \quad (2.53)$$

The values of the dimensionless parameters (λ^2, a^2) can vary, depending on the dielectric permittivity, the reference number density, the reference pressure and reference length.

For the following, meaningful, physical values

$$T = 293.75[\text{K}] \quad (2.54)$$

$$n^{\text{ref}} = 55[\text{mol/l}] = 55 \cdot N_A \cdot 10^{-3}[\text{l/m}^3] \quad (2.55)$$

$$p^{\text{ref}} = 1[\text{atm}] = 1.01325 \cdot 10^5[\text{Pa}] \quad (2.56)$$

$$L^{\text{ref}} = 20[\text{nm}] = 20 \cdot 10^{-9}[\text{m}] \quad (2.57)$$

$$\chi = 80[-] \quad (2.58)$$

one ends up with

$$\lambda^2 = 8.553 \cdot 10^{-6} \quad (2.59)$$

$$a^2 = 7.5412 \cdot 10^{-4} \quad (2.60)$$

The values for T , n^{ref} , p^{ref} and χ are taken from [2]. As there could not be found the length of the full domain, which was used, L^{ref} set to 20nm, as this length could be found in [7]. These values are used in the remaining parts, if not explicitly stated otherwise.

Chapter 3

One-Dimensional Equilibrium

Reducing the dimensions to one dimension and considering only the equilibrium case, $\mathbf{J}_\alpha = 0$, $\nabla\mu_N = 0$ [3], the atomic fractions can be expressed in dependence of the electric potential and the pressure. This reduces the number of equations from $N + 1$ to only two equations.

$$0 = \mathbf{J}_\alpha = \partial_x(\mu_\alpha + z_\alpha\varphi) \quad (3.1)$$

$$= \partial_x \left(g_\alpha^{\text{ref}} + (\kappa + 1)a^2K \ln \left(1 + \frac{1}{K}(p - 1) \right) + \ln(y_\alpha) + z_\alpha\varphi \right) \quad (3.2)$$

$$= (\kappa + 1)a^2 \frac{K}{K + p - 1} \partial_x p + \partial_x \ln(y_\alpha) + z_\alpha \partial_x \varphi \quad (3.3)$$

$$\Leftrightarrow \partial_x \ln(y_\alpha) = -(\kappa + 1)a^2 \frac{K}{K + p - 1} \partial_x p - z_\alpha \partial_x \varphi \quad (3.4)$$

$$\Leftrightarrow \ln(y_\alpha) = -(\kappa + 1)a^2K \ln(K + p - 1) - z_\alpha\varphi + \tilde{C}_\alpha \quad (3.5)$$

$$\Leftrightarrow y_\alpha = \exp \left(-(\kappa + 1)a^2K \ln(K + p - 1) - z_\alpha\varphi + \tilde{C}_\alpha \right) \quad (3.6)$$

$$= C_\alpha (K + p - 1)^{-(\kappa+1)a^2K} \exp(-z_\alpha\varphi) \quad (3.7)$$

with the constant of integration, C_α . Plugging the boundary values on the right side of the domain ($*^R$) into the formula, representing the inner side of the electrolyte, one gets

$$C_\alpha = \frac{y_\alpha^R}{(K + p^R - 1)^{-(\kappa+1)a^2K} \exp(-z_\alpha\varphi^R)} \quad (3.8)$$

$$y_\alpha(\varphi, p) = \frac{y_\alpha^R (K + p - 1)^{-(\kappa+1)a^2K} \exp(-z_\alpha\varphi)}{(K + p^R - 1)^{-(\kappa+1)a^2K} \exp(-z_\alpha\varphi^R)} \quad (3.9)$$

with this taken into account, the two remaining equations, needed to be solved, are

$$\lambda^2 \partial_{xx} \varphi = -n^F \quad (3.10)$$

$$a^2 \partial_x p = -n^F \partial_x \varphi \quad (3.11)$$

3.1 Incompressible Limit

As already discussed, an incompressible mixture is defined by $K \rightarrow \infty$.

For this case, the expression for the atomic fractions is simplified to

$$0 = \mathbf{J}_\alpha = \partial_x(\mu_\alpha + z_\alpha \varphi) \quad (3.12)$$

$$= \partial_x (\ln(y_\alpha + (\kappa + 1)a^2(p - 1) + z_\alpha \varphi)) \quad (3.13)$$

$$\Leftrightarrow \partial_x \ln(y_\alpha) = -(\kappa + 1)a^2 \partial_x p - z_\alpha \partial_x \varphi \quad (3.14)$$

$$\Leftrightarrow \ln(y_\alpha) = -(\kappa + 1)a^2 p - z_\alpha \varphi + \tilde{D}_\alpha \quad (3.15)$$

$$\Leftrightarrow y_\alpha = D_\alpha \exp(-(\kappa + 1)a^2 p - z_\alpha \varphi) \quad (3.16)$$

with D_α as the integration constant. Once more, the boundary values on the right side of the domain are plugged into the formula for the atomic fractions.

$$D_\alpha = \frac{y_\alpha^R}{\exp(-(\kappa + 1)a^2 p^R - z_\alpha \varphi^R)} \quad (3.17)$$

$$y_\alpha(\varphi, p) = \frac{y_\alpha^R \exp(-(\kappa + 1)a^2 p - z_\alpha \varphi)}{\exp(-(\kappa + 1)a^2 p^R - z_\alpha \varphi^R)} \quad (3.18)$$

3.2 Neglecting the Pressure Dependency

Assume that the spatial derivative of the electric potential inside the electrolyte is vanishing ($\partial_x \varphi^R = \epsilon \ll 1$). Under this condition, the pressure can be expressed in terms of the electric potential by plugging 3.10 into 3.11

$$a^2 \partial_x p = -n^F \partial_x \varphi \quad (3.19)$$

$$\partial_x p = -\frac{n^F}{a^2} \partial_x \varphi = \frac{\lambda^2}{a^2} \partial_{xx} \varphi \partial_x \varphi \quad (3.20)$$

$$\Rightarrow p = \frac{1}{2} \frac{\lambda^2}{a^2} (\partial_x \varphi)^2 + E_p \quad (3.21)$$

Inserting the vanishing derivative of the electric potential inside the electrolyte, in this case assumed to be on the right side of the domain, the constant of integration, E_p , reads

$$E_p = p^R \quad (3.22)$$

Only equation 3.10 remains to be solved.

3.3 The Charge of the System

!!!ToDo: Only working for $\kappa = 0$ currently, as $\kappa_N = 0, \kappa_\alpha = \kappa$ for $\alpha = 1, \dots, N - 1$ + Do it for compressible-case, if possible!!!

The charge, stored in the system, can be identified as (see [9, 13])

$$Q_{dl} = \int_{\Omega} n^F dx \quad (3.23)$$

Under the assumption, that the mixture is in equilibrium, incompressible with a vanishing derivative of the electric potential at the right boundary and in one spatial domain, this integral can be calculated analytically.

Recall equation 3.10

$$n^F = -\lambda^2 \partial_{xx} \varphi \quad (3.24)$$

$$\Rightarrow Q_{dl} = \int_{\Omega} n^F dx = \int_{\Omega} -\lambda^2 \partial_{xx} \varphi dx \quad (3.25)$$

$$= \lambda^2 (\partial_x \varphi^L - \partial_x \varphi^R) \quad (3.26)$$

With the knowledge, that the atomic fractions over all species sum up to one

$$1 = \sum_{\alpha=1}^N y_{\alpha} = \sum_{\alpha=1}^N D_{\alpha} \exp \left(-(\kappa + 1) \frac{1}{2} \lambda^2 (\partial_x \varphi)^2 + E_p a^2 - z_{\alpha} \varphi \right) \quad (3.27)$$

$$= \sum_{\alpha=1}^N D_{\alpha} \exp(-z_{\alpha} \varphi + E_p a^2) \exp \left(-(\kappa + 1) \frac{1}{2} \lambda^2 (\partial_x \varphi)^2 \right) \quad \Big| \ln(\cdot) \quad (3.28)$$

$$\Leftrightarrow 0 = \ln \left(\underbrace{\sum_{\alpha=1}^N D_{\alpha} \exp(-z_{\alpha} \varphi + E_p a^2)}_{\Lambda} - (\kappa + 1) \frac{1}{2} \lambda^2 (\partial_x \varphi)^2 \right) \quad (3.29)$$

$$\Leftrightarrow \partial_x \varphi = \pm \sqrt{\frac{2}{\lambda^2} \frac{\Lambda}{\kappa + 1}} \quad (3.30)$$

where expression 3.16 was used and expression 3.21 was reformulated to $a^2 p$ and inserted. Taking into account knowledge of the system, due to different simulations, it is known that the electric potential increases or decreases monotonously. **Change this to explanation, that $\partial_x \varphi$ is now known and Λ has same sign, so $\partial_x \varphi$ is increasing monotonously. Ausarbeit!!!**

This yields

$$\partial_x \varphi = \begin{cases} \sqrt{\frac{2}{\lambda^2} \frac{\Lambda}{\kappa + 1}} & , \varphi^L - \varphi^R > 0 \\ 0 & , \varphi^L = \varphi^R \\ -\sqrt{\frac{2}{\lambda^2} \frac{\Lambda}{\kappa + 1}} & , \varphi^L - \varphi^R < 0 \end{cases} \quad (3.31)$$

Finally, the charge of the system can be calculated as

$$Q_{dl} = \text{sgn}(\varphi^L - \varphi^R) \lambda \sqrt{\frac{2}{\kappa + 1}} \left(\sqrt{\Lambda^L} - \sqrt{\Lambda^R} \right) \quad (3.32)$$

Chapter 4

Numerical Implementation

The system of coupled nonlinear partial differential equations (2.44-2.46) was solved numerically, with the finite element method.

The open source computing platform FEniCS¹ (in this work referred as FEniCS or fenics) was used. FEniCS is a collection of different software to solve partial differential equations. It consists of the packages DOLFINx, FFCx, Basix and UFL and offers high level Python and C++ interfaces.

FEniCS's goal is to enable researchers to quickly and efficiently translate mathematical models into finite element code. Therefore, the user needs to define the variational formulation of the problem, the function spaces, finite elements, boundary conditions and the grid. FEniCS then automatically finds a numerical solution to the variational formulation. The user has no need to implement finite elements, assembly, the solver or anything else by hand.

The implementation and all the shown examples and visualizations can be found in the repository [11].

4.1 Variational Formulation

The numerical solution is based on a mixed finite element formulation with a set of standard scalar Lagrange finite elements of degree one.

The definition of finite elements is based on the Sobolev space. The general definition for the Sobolev space of order m is

$$H^m(\Omega) = \{u \in L^2(\Omega) : D^i u \in L^2(\Omega) \text{ for all } i \in \mathbb{N}_0^n \text{ with } |i| \leq m\} \quad (4.1)$$

with the spatial domain $\Omega \subset \mathbb{R}^n$, the number of dimensions n , $D^i u$ the i -th derivative of u , the constraint $m \geq 1$ and the L^2 norm. [12].

$$L^2(\Omega) = \{f : \Omega \rightarrow \mathbb{R}, \text{ Lebesgue-integrable, } \int_{\Omega} |f(x)|^2 dx < \infty\} \quad (4.2)$$

For the dimensionless system of partial differential equations, the domain simplifies to $\Omega \in [0, 1]^n$, $1 \leq n \leq 3$ and the domain's boundary is $\partial\Omega$. The boundary consists of Dirichlet (Γ_D) and Neumann (Γ_N) boundary conditions

$$\partial\Omega = \Gamma_D \cup \Gamma_N \quad (4.3)$$

The function space of the trial functions is defined as follows

$$V = \{u \in H^1(\Omega) | u = u_D \text{ on } \Gamma_D\} \quad (4.4)$$

and the function space of the test functions is

¹<https://fenicsproject.org/>

$$\hat{V} = \{u \in H^1(\Omega) | u = 0 \text{ on } \Gamma_D\} \quad (4.5)$$

With this kept in mind, the variational formulation for the whole system is

$$0 = \int_{\Omega} \nabla \varphi \cdot \nabla v_{\varphi} d\Omega - \int_{\Gamma_N} g_{\varphi} v_{\varphi} ds - \int_{\Omega} \frac{1}{\lambda^2} n^F d\Omega \quad (4.6)$$

$$+ \int_{\Omega} \left(\nabla p + \frac{1}{a^2} n^F \nabla \varphi \right) \cdot \nabla v_p d\Omega - \int_{\Gamma_N} g_p v_p ds \quad (4.7)$$

$$+ \sum_{\alpha=1}^{N-1} \left(\int_{\Omega} \mathbf{J}_{\alpha} \cdot \nabla v_{y_{\alpha}} - \int_{\Gamma_N} g_{y_{\alpha}} v_{y_{\alpha}} ds \right) \quad (4.8)$$

$d\Omega$ defines the volume integral and ds the line integral. The Neumann boundary conditions are formulated as

$$g_{\varphi} = \lambda^2 \nabla \varphi \cdot \vec{n} \quad (4.9)$$

$$g_p = \left(\nabla p + \frac{1}{a^2} n^F \nabla \varphi \right) \cdot \vec{n} \quad (4.10)$$

$$g_{y_{\alpha}} = \mathbf{J}_{\alpha} \cdot \vec{n} \quad \alpha \in \{1, \dots, N-1\} \quad (4.11)$$

\vec{n} denotes the outward unit normal. If not explicitly stated, only homogeneous Neumann boundary conditions ($g_{\varphi} = g_p = g_{y_{\alpha}} = 0$ for $\alpha \in \{1, \dots, N-1\}$) are used in this work.

The unknowns are $(\varphi, p, y_{\alpha}) \in [V]^{N+1}$ and the corresponding test functions $(v_{\varphi}, v_p, v_{y_{\alpha}}) \in [\hat{V}]$ for $\alpha \in \{1, \dots, N-1\}$. Note that the space charge n^F is a function of y_{α} for $\alpha \in \{1, \dots, N-1\}$ and the flux \mathbf{J}_{α} of species α is a function of the electric potential, pressure and the corresponding atomic fraction of species α . A detailed derivation of the variational formulation can be found in Appendix 5.9.1.

For the one dimensional equilibrium case, as discussed in chapter 3, the variational formulation reduces to the first two lines of equation 4.1 to solve for the electric potential and pressure. With the assumptions from section 3.2 it even reduces to the very first line.

4.2 Numerical Treatment of Nonlinearity

- **ToDo**
 - Explain Newton
 - Relaxation (Damping)
 - Evtl. constraints for Newton with backtracking, self defined Newton, ...
 - Explain what was not working
 - * Multigrid
 - * Continousmethod

4.3 Validation

- Insert picture with dim-values from Dreyer paper
 -
- Explain validation with DLKap

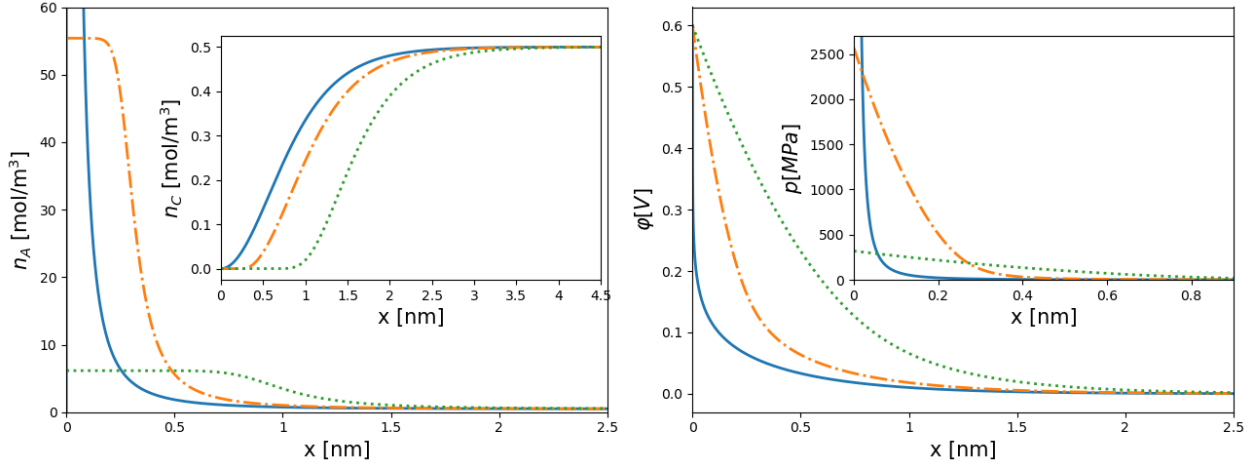


Figure 4.1: Placeholder -> Update with *.svg, analyze while x-scaling wrong, write texts

4.4 Convergence

To ensure the correctness of the numerical implementation, a convergence analysis was performed. Since there is no known analytical solution for the system of equations, the results for different grid sizes will be compared to the solution of a very fine grid.

Error Measures To interpret the convergence of the numerical method, relevant error measures are introduced.

The L_2 norm is calculated as

$$L_2(\Omega) = \int_{\Omega} (f_{\text{fine}} - f_h)^2 d\Omega \quad (4.12)$$

with f_{fine} the solution on the finest available grid.

The infinity norm is introduced as

$$L_{\infty}(\Omega) = \max_{n \in \eta} \left(\left| f_{\text{fine}} - f_h \right| \right)_{\eta} \quad (4.13)$$

with η the set of all mesh nodes. In case that the infinity norm converges towards zero, the solution converges towards the exact solution on all node values.

The convergence analysis was done on a one dimensional, ternary, incompressible electrolyte with an applied potential difference of 6.0 ($\delta\varphi = \varphi^R - \varphi^L$), a vanishing pressure on the right side of the domain and a share of $\frac{1}{3}$ for each constituent at the right boundary, $\lambda^2 = 8.33 \cdot 10^{-8}$ and $a^2 = 7.3656 \cdot 10^{-4}$. The solutions were compared to the solution on a grid with element size $h = 1 \cdot 10^{-6}$.

Figure 4.2 shows the convergence of the numerical implementation. On the x-axis, the element size, h , is visualized. Since the calculations were performed on a uniform, one dimensional grid, the element size is the distance between two neighboring nodes and the same for all elements. The y-axis shows the calculated error with the L_2 norm on the left and the infinity norm on the right of Figure 4.2. Both axis are scaled logarithmic.

The numerical method converges towards zero in both error norms. Therefore, the solution converges towards the exact solution over the whole domain and on each node point, too.

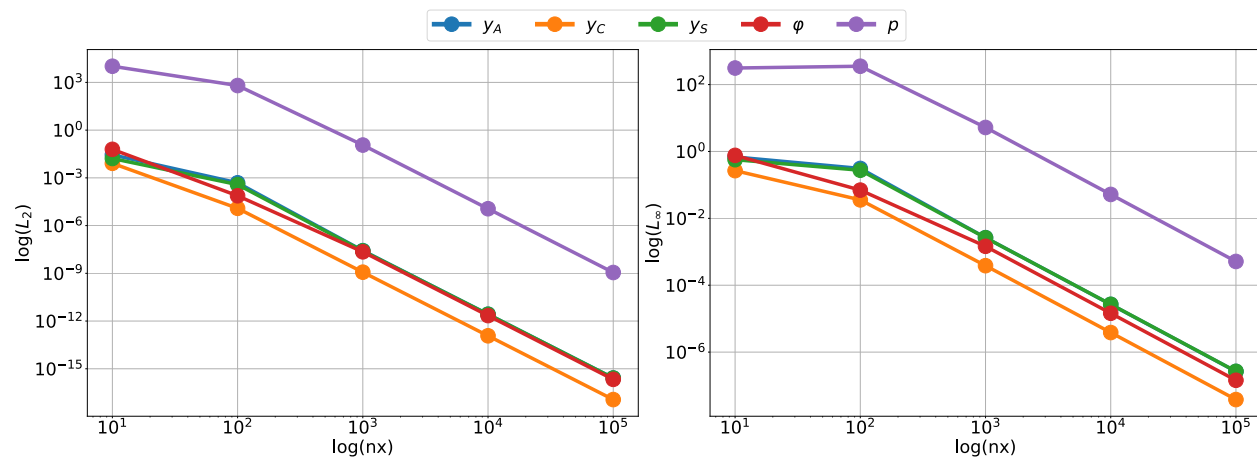


Figure 4.2: Convergence

Chapter 5

Results

All numerical results, besides those presented in section 5.2, are calculated with the finite element method in FEniCS, as discussed in chapter 4.

Furthermore, if not other stated, the mixture is assumed to be incompressible and the solvation effect is neglected. Compressibility will be inspected in section 5.6 and solvation in section 5.5. If a ternary electrolyte is presented (sections 5.1 - 5.7.3 and section 5.9.1), the charge numbers are

$$z_A = -1 \tag{5.1}$$

$$z_C = 1 \tag{5.2}$$

$$z_N = 0 \tag{5.3}$$

Besides section 5.9.1 only homogeneous Neumann boundary conditions are applied.

5.1 Ternary Electrolyte

For a very first impression of the solution, an incompressible, ternary mixture with the default dimensionless quantities $\lambda^2 = 8.553 \cdot 10^{-6}$ and $a^2 = 7.5412 \cdot 10^{-4}$ was used with the following boundary conditions

$$\begin{aligned} \varphi^L &= 0.0, & \varphi^R &= 8.0 \\ p^R &= 0.0, & y_A^R &= y_C^R = \frac{1}{3} \end{aligned}$$

The domain describes the boundary layer of the electrolyte, with the inner point of the electrolyte somewhere far away from the right side of the domain. In the inside of the electrolyte, the electric potential, pressure and all three atomic fractions are described by Dirichlet boundary conditions. Only $x_{\text{vis}} = [0, 0.05]$ from the computational domain $x = [0, 1]$ is visualized, as the solution is constant on the remaining part of the domain.

Figure 5.1 shows a first result for a one dimensional ternary electrolyte. The x-axis represents the spatial domain and the y-axis the corresponding value for each property. On the left side, the electric potential (blue line, left axis) and the pressure (red line, right axis) can be found. The right side shows the atomic fractions (blue lines, left axis) and the space charge (red line, right axis). The vertical green line indicates the point where the space charge first diverges from zero, coming from the right side of the domain.

The boundary conditions force the fractions of all species to be evenly distributed in the inner of the electrolyte, which leads to local charge neutrality ($n^F|_{x=1} = (z_A y_A^R + z_C y_C^R)|_{x=1} = 0$), which is conserved over a large part of the domain. Getting closer to the boundary, these atomic fractions are diverging from each other. The number of negatively charged anions increases, while the number of positively charged cations and the neutral solvent decreases. The increase and decrease stop at the values of zero and one, preventing the system from engaging in nonphysical behavior. Therefore, the anions share reaches its saturation point at the value of one, while the cations and neutral solvents share have their saturation point at the value of zero. Once reaching this saturation point, the fractions remain constant.

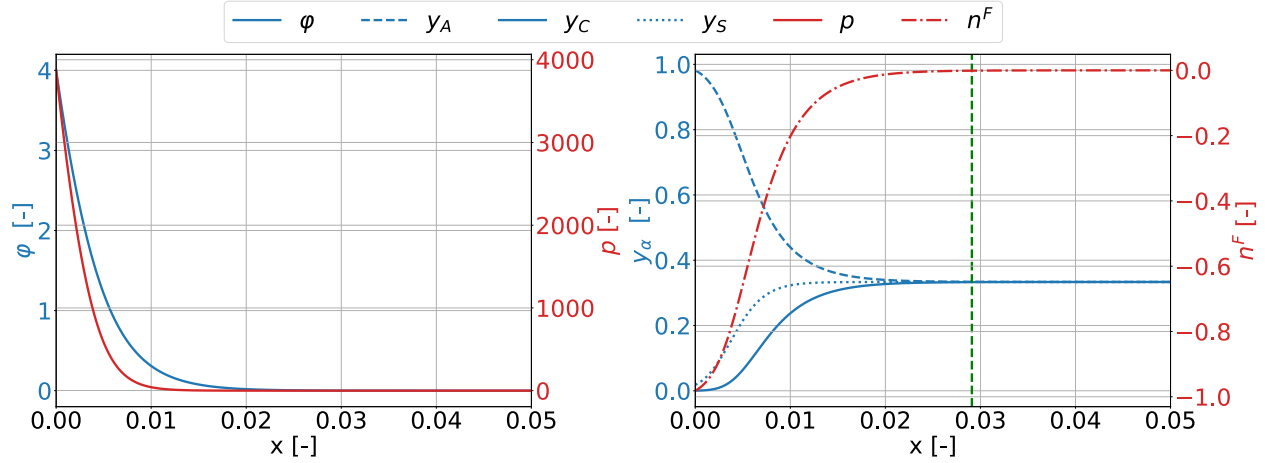


Figure 5.1: Ternary electrolyte

Additionally, the neutral solvent needs a larger part of the domain till it reaches the lower boundary value, compared to the cations. The value of cations is closer to zero as the value of anions to one and the neutral solvents share is computed as the remaining fraction of the mixture. Finally, on the left side of the domain, the mixture almost only consists of anions, and nearly no cations and solvent particles can be found there.

Furthermore, from the point where the values of the atomic fractions start to diverge, the free charge density, n^F , gets unequal to zero. This also initializes the first change in the electric potential, due to the relation of the space charge to the Laplace operator of the electric potential in equation 2.44.

The blocking for the fractions to go beyond the range of $[0, 1]$ is an achievement of the thermodynamically consistent coupling of the DGM model. In the classical Nernst-Planck model, there is no such blocking leading to a nonphysical behavior, as it will be discussed in section 5.4.

5.2 One-Dimensional Equilibrium - An Instructive Example

Again, an incompressible, ternary electrolyte ($\alpha \in \{A, C\}$) is taken into account, as discussed in section 2.7. Furthermore, the mixture is assumed to be in equilibrium ($\mathbf{J}_\alpha = 0$ for $\alpha \in \{A, C\}$, $\nabla \mu_N = 0$, compare with [3]) and the pressure dependency is neglected by the assumption that the derivative of the electric potential on the right side of the domain is very small ($\nabla \varphi^R \ll 1$, see chapter 3). The domain is reduced to one dimension ($\tilde{\Omega} \in [-L_x, 0]$, $L_x \in \mathbb{R}^+$, leading to a change in notation for the derivatives ($\nabla \cdot \rightarrow \partial_x \cdot$). A single ordinary differential equation of order two remains to be solved

$$\partial_{xx}\varphi = -\frac{1}{\lambda^2}n^F \quad (5.4)$$

Reformulating this equation into a system of ordinary differential equations of order one leads to

$$\partial_x \varphi = \phi \quad (5.5)$$

$$\partial_x \phi = -\frac{1}{\lambda^2}n^F \quad (5.6)$$

The initial values are chosen as:

$$\varphi(0) = 0 \quad (5.7)$$

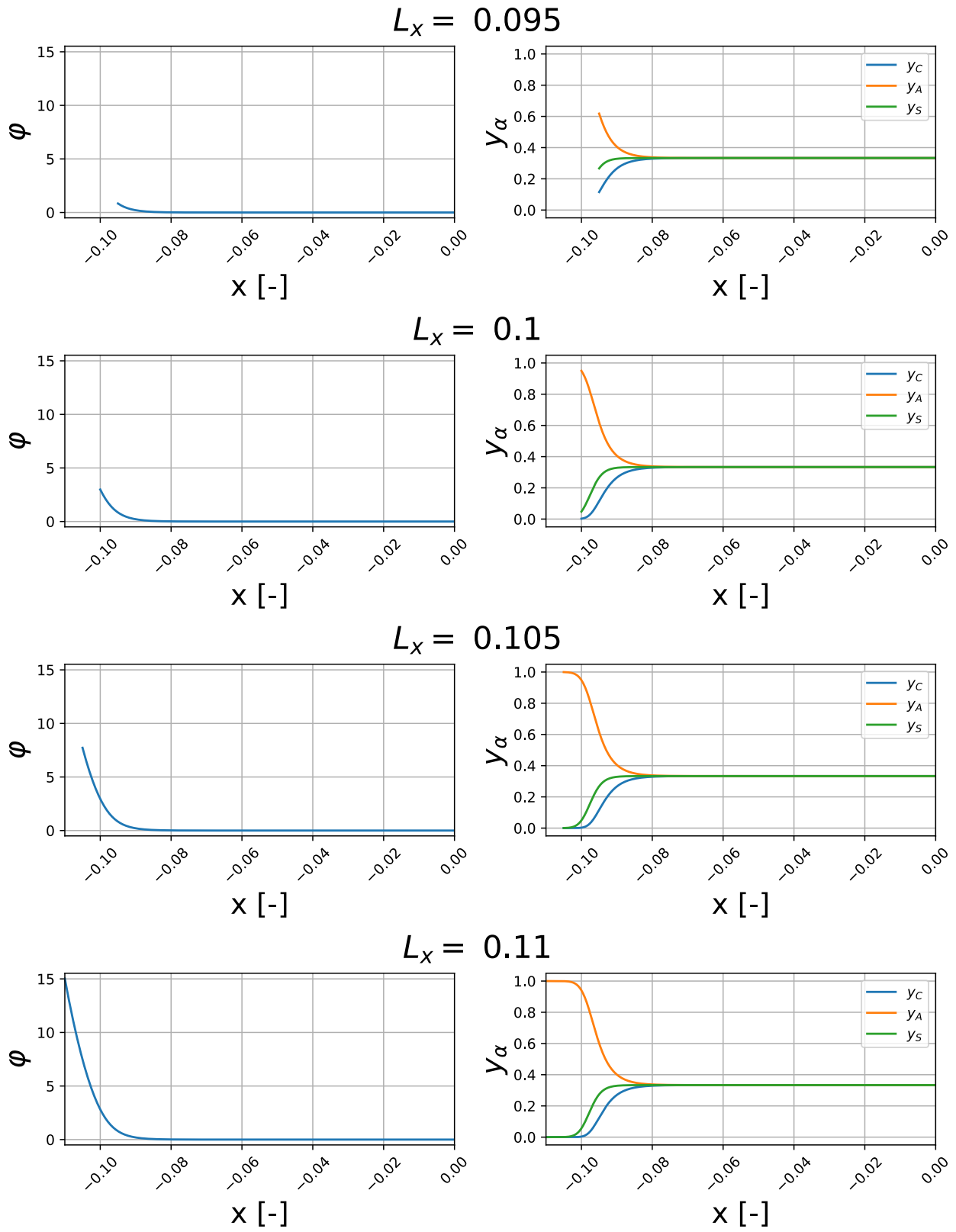
$$\phi(0) = \epsilon \ll 1 \quad (5.8)$$

with

$$y_A^R = y_C^R = \frac{1}{3} \tag{5.9}$$

to determine the constants of integration for the semi-analytic expression for the atomic fractions.

This system is finally solved with the python package “SciPy”, especially with the very simple `odeint` function. The results are visualized on different length scales of the domain $\tilde{\Omega}$ and can be found in Figure 5.2.

Figure 5.2: Solutions for different L_x with $\lambda^2 = 1 \cdot 10^{-3}$, $z_A = -1$, $z_C = 1$

One can see, that the assumption ($\partial_x \varphi^L = \phi^L \ll 1$) does not change the behavior of the system (compare with Figure 5.1). Local charge neutrality, enforced by the boundary conditions on the right side of the domain, is conserved over a major part of $\tilde{\Omega}$. Then, the anion's distribution starts to rise, while the cations and neutral solvent's distribution starts to fall. The blocking at the values of zero and one can be observed. The electric potential is constant over a large part of the domain and starts to increase exponentially, on the left side.

In this instructive example, it can be further verified that the length of the domain behaves the same as a Dirichlet boundary condition. Increasing the length from L_{x1} on $\tilde{\Omega}_1$ to L_{x2} on $\tilde{\Omega}_2$ neither the electric potential nor any atomic fraction changes in the part of the smaller domain L_{x1} for the new, larger domain L_{x2} . This means that, as long as a point x_1 is inside the computational domain $\tilde{\Omega}_1$, the solution at x_1 is the same, independent from the size of $\tilde{\Omega}_1$.

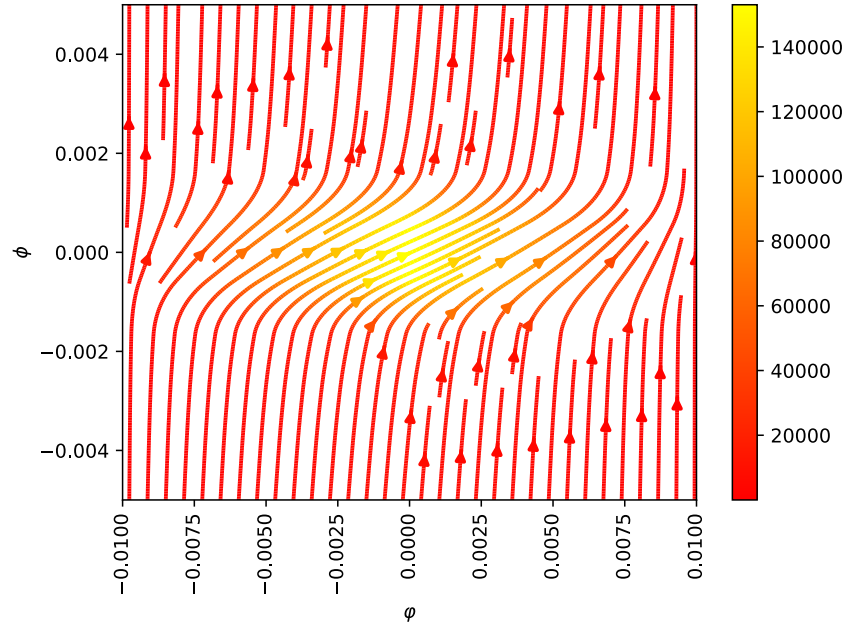


Figure 5.3: Streamplot of the solution at the left-most point for the electric potential

The streamplot in Figure 5.3 visualizes different starting points for the electric potential (φ) and its derivative (ϕ) on the domain $\tilde{\Omega} = [-1.5 \cdot 10^{-2}, 0]$ with 1024 points. The visualized value is the derivative of the electric potential with respect to the initial values of φ and ϕ . The value ϕ has a huge impact on the solution. The smaller the value is chosen, the larger is the part of the domain where local charge neutrality can be observed. The smaller the value is chosen, the more space is needed for the ion distribution to diverge. Setting the value to zero will lead to a constant solution for the electric potential and ion distribution.

5.3 Analysis of Parameter

To understand the behavior of the ternary electrolyte in the boundary layer, it is crucial to understand the influence of each parameter on the solution.

Solutions for varying dimensionless parameters (λ^2, a^2) with a varying potential difference ($\delta\varphi = \varphi^L - \varphi^R$) will be presented in the following. An incompressible mixture with the following boundary conditions is used for all solutions

$$\begin{aligned} \varphi^R &= 0.0 & p^R &= 0.0 \\ y_\alpha^R &= \frac{1}{3} \text{ for } \alpha \in \{A, C\} \end{aligned}$$

The solutions will be only visualized on a part ($x_{\text{vis}} = [0, 0.08]$) of the whole computational domain ($x = [0, 1]$), as the solution is constant on the remaining part of the domain.

5.3.1 Electric Potential and Pressure

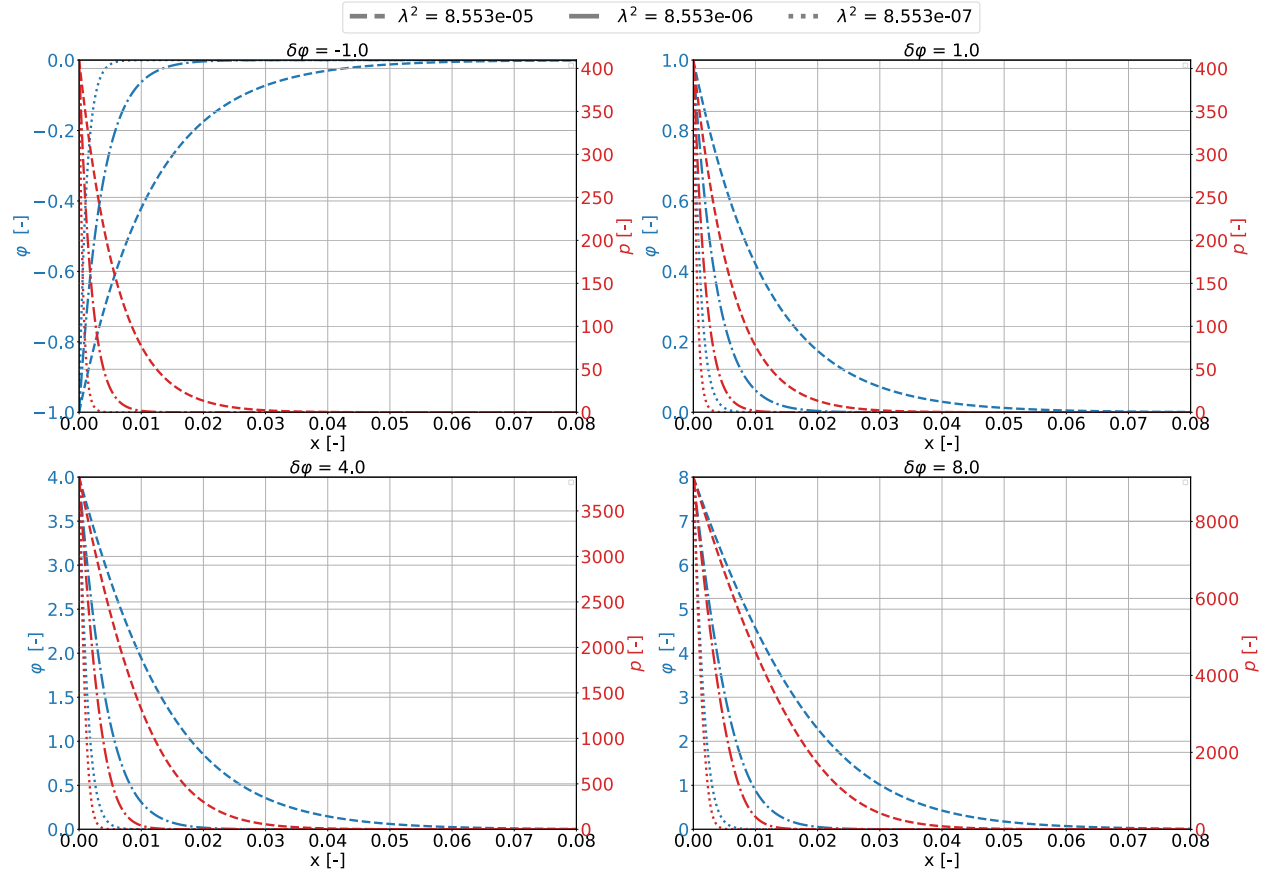


Figure 5.4: Influence of the potential difference and the dimensionless parameter λ on the electric potential and the pressure

Figure 5.4 visualizes the influence of λ^2 and the applied potential difference on the electric potential (blue lines, left axis) and the pressure (red lines, right axis). The dimensionless parameter a^2 was fixed to $7.5412 \cdot 10^{-4}$. The parameter λ^2 can be identified to be a scaling parameter for the electric potential and the pressure. Increasing the value leads to a more bulbous shape while decreasing it leads to a sharper shape. The parameter has also neither an influence on the range of the solution space nor on the free boundary value for the pressure at the left side p^L .

This value is influenced by the applied potential difference. Enforced due to the boundary conditions, a larger potential difference leads to a larger solution space for the electric potential, but also to the pressure. A negative potential difference flips the solution for the electric potential, (compare $\delta\varphi = -1.0$ to $\delta\varphi = 1.0$), while the sign of the applied potential difference does not influence the solution for the pressure. The potential difference indicates to have no impact on the shape of the solution, but just enlarges the range of it. This phenomenon is further inspected in Figure 5.5.

Four different, positive, potential differences are applied, with the default values for λ^2 and a^2 . On the left side, the numerical solution for the electric potential can be found and is scaled to the applied potential difference, on the right side. This scaling does not lead to the same results. Therefore, the applied potential difference does not only act as a scaling parameter for the electric potential.

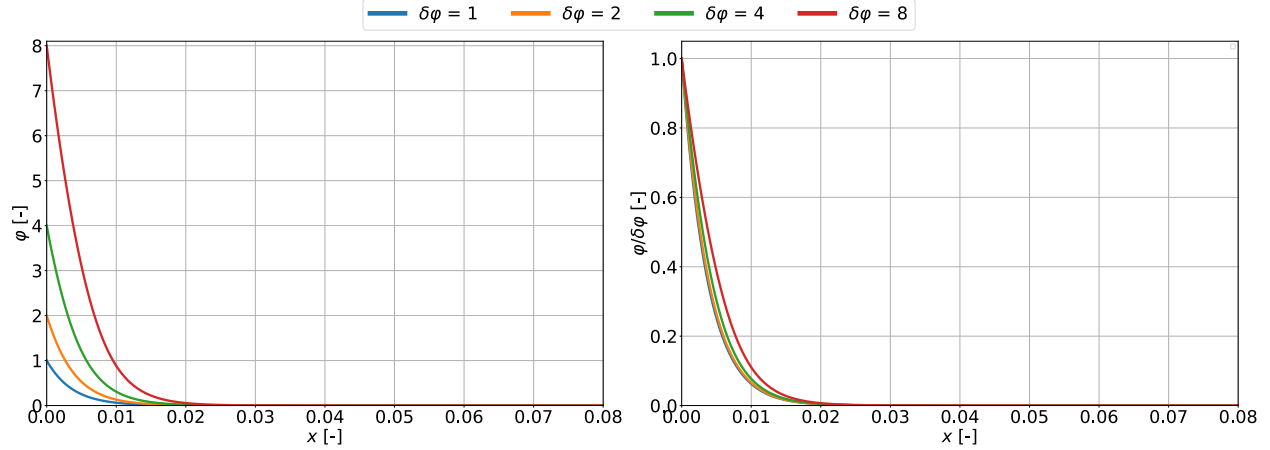


Figure 5.5: Scaling of the electric potential

5.3.2 Atomic Fractions

Figure 5.6 visualizes the influence of the parameter λ^2 and the applied potential difference on the atomic fractions. The dashed lines show the anions fractions, the solid lines the cations fractions and the dotted lines the fractions of the neutral solvent. Furthermore, the color indicates the size of λ^2 while each figure shows a different applied voltage difference ($\delta\varphi = 0.1$ top left, $\delta\varphi = 1.0$ top right, $\delta\varphi = 4.0$ bottom left, $\delta\varphi = 8.0$ bottom right).

Once more, the parameter λ^2 can be verified as decisive for the shape of the solution. A smaller value, as indicated in green, leads to a sharper shape, while a larger value, blue, leads to a more bulbous shape. Therefore, λ^2 can be identified as a scaling parameter for the atomic fractions.

The share of anion particles tends to increase, from inside the electrolyte to the boundary (right to left), when applying a positive potential difference, while the fractions of the cations and the neutral solvent particles tend to decrease. For an applied negative potential difference, the share of cation particles increases, from right to left, while the anions and neutral solvents share decreases. The fractions do not reach their saturation point for rather small potential differences, and therefore also do not show the blocking at the range of $[0, 1]$.

For a potential difference of 4.0, the cations fractions can be observed to be blocked to go beyond zero. On the other hand, the anions get very close to the upper boundary of one but do not reach it. However, the gradient is starting to decrease, close to the boundary, indicating this blocking behavior of the system. Increasing the potential difference to 8.0, the expected blocking behavior at the range of $[0, 1]$ can be observed.

Dependence of the dimensionless parameter a Till now, only the dependence of the potential difference and the dimensionless quantity λ^2 was inspected. The parameter a^2 has an impact on the pressure, but neither on the electric potential nor the atomic fractions.

ToDo: Change notation to scientific one

In Figure 5.3.2 the influence of different values for a^2 (indicated by different colors) can be verified. The potential difference was set to 8.0 and λ^2 to its default value. The solution indicates that a decreasing value of a^2 (indicated by the green line) leads to a larger difference in the pressure and a larger maximum pressure value, while a larger value for a^2 leads to a smaller pressure difference.

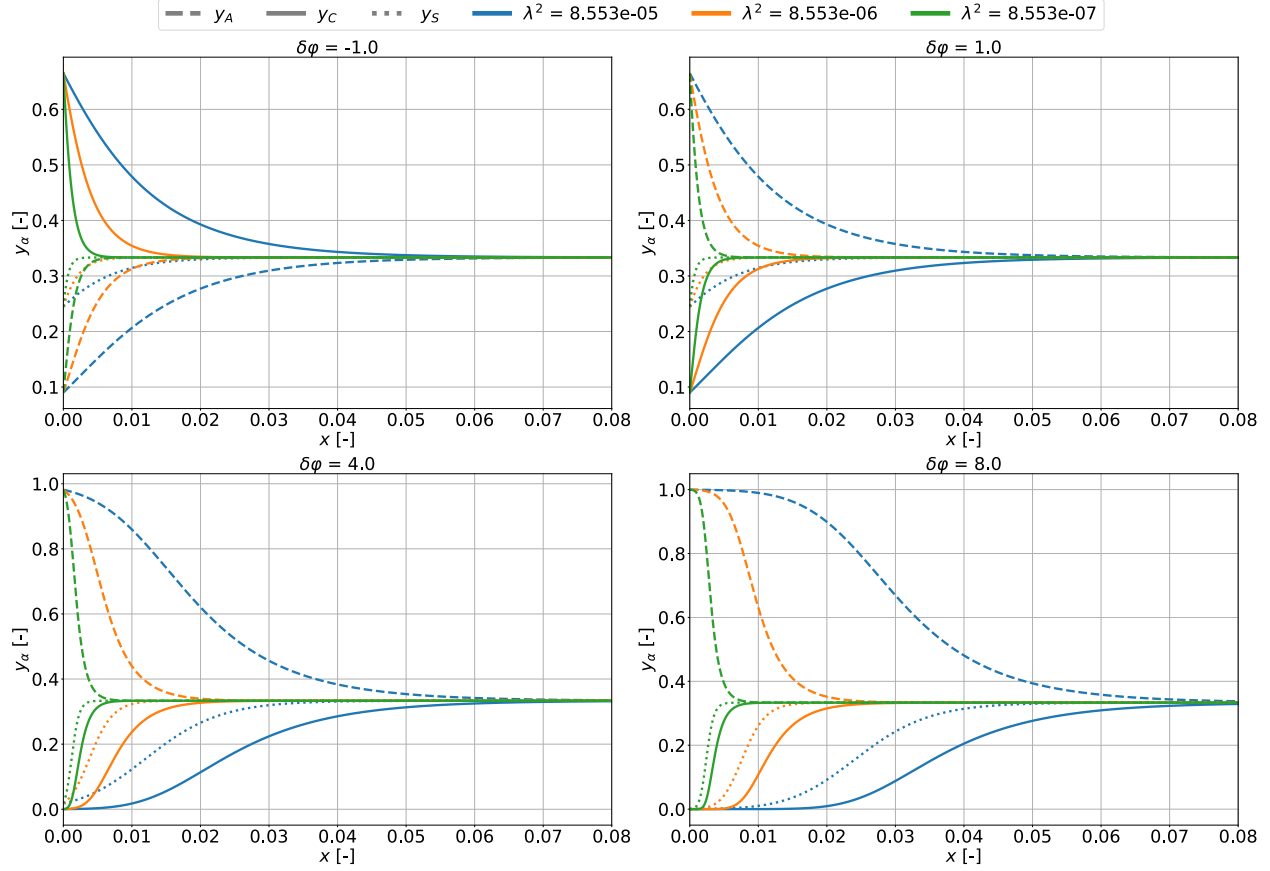


Figure 5.6: Influence of the potential difference and the dimensionless parameter λ on the atomic fractions

5.4 Comparison to classical Nernst-Planck model

The thermodynamically consistent model neglects some key drawbacks from the classical Nernst-Planck/Poisson-Boltzmann theory. First, the DGM model takes into account the right coupling of fluxes, as there are only $N - 1$ independent fluxes and the n -th flux is calculated from the side condition

$$\sum_{\alpha=1}^N J_{\alpha} = 0 \quad (5.10)$$

which then splits the partial mass balances into $N - 1$ diffusion equations, as discussed in chapter 2. Furthermore, the classical Nernst-Planck model fails to couple the diffusion fluxes to the pressure term and to the interaction with the chemical potential of the neutral solvent. Therefore, in the one dimensional equilibrium case, the atomic fractions of the Nernst-Planck model are proportional to the exponent of the negative charge number multiplied by the electric potential and do not reach any saturation at the range of $[0, 1]$ which can lead to nonphysical results.

The following comparison to the classical Nernst-Planck model was performed on an incompressible, ternary electrolyte with the following boundary conditions

$$\begin{aligned} \varphi^R &= 0.0, & p^R &= 0.0 \\ y_{\alpha}^R &= \frac{1}{3} \text{ for } \alpha \in \{A, C\} \end{aligned}$$

The electric potential on the left side, φ^L , is varied between different values with the default values for λ^2 and a^2 .

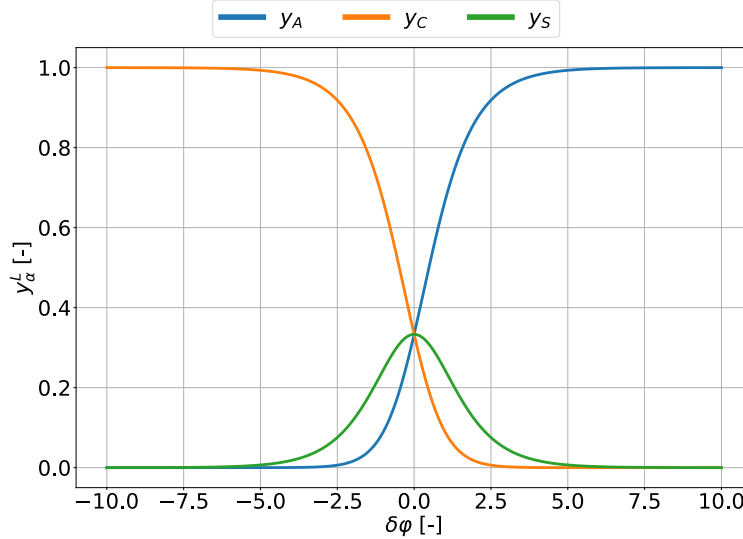


Figure 5.7: Value of the atomic fractions at the left boundary for different applied voltage differences

As already inspected in section 5.3, a large applied potential difference drives the atomic fractions to their boundary values of zero and one, in the DGM model. On the other hand, the classical Nernst-Planck model has no such blocking. For large enough potential differences the atomic fractions go beyond the range of zero and one and therefore become nonphysical. Comparing the mathematical formulation of both models in the one dimensional equilibrium, the Nernst-Planck model is described by the Poisson-Boltzmann (PB) formulation for a one-dimensional mixture in equilibrium,

$$y_{\alpha}^{\text{DGM}} \propto \exp(-z_{\alpha}\varphi + a^2 p) \quad (5.11)$$

$$y_{\alpha}^{\text{PB}} \propto \exp(-z_{\alpha}\varphi) \quad (5.12)$$

the coupling with the pressure term in the exponent can be identified as crucial to block the ions from going beyond the range of $[0, 1]$ as the anion share for the Poisson-Boltzmann formulation goes beyond the upper limit of one. For the cations share, the distribution over the whole domain may be wrong, since the shape of it is more flat, compared to the DGM model, but it is blocked from going beyond zero. The neutral solvent, on the other hand, has also negative fractions and therefore reaches a nonphysical behavior.

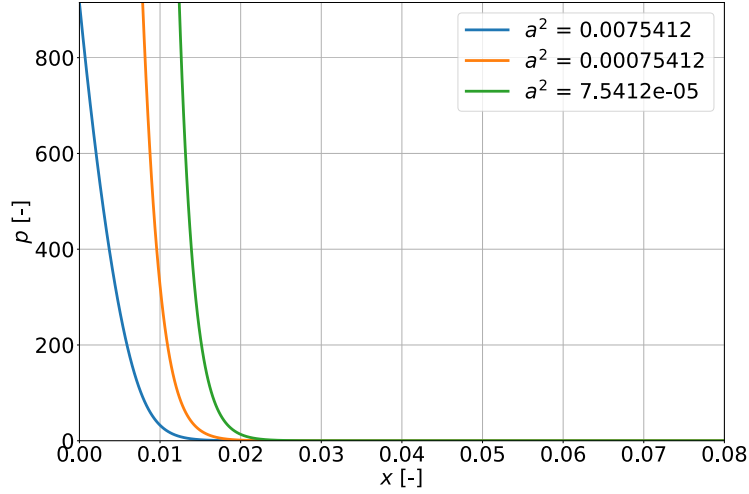
Furthermore, it can be inspected that for rather small potential differences, the Nernst-Planck model is a good approximation of the DGM model.

Figure 5.10 shows the relation between the error of the Poisson-Boltzmann formulation, compared to the DGM model, for different applied voltage differences. The x-axis shows the applied voltage difference while the y-axis shows the error from the Poisson-Boltzmann formulation. The error is calculated in the L_2 norm on the left side and in the infinity norm (L_{∞}) on the right side and computed separately for each species.

The smaller the applied voltage difference, the better the approximation of the Nernst-Planck model to the DGM model. In the L_2 norm, the error for the atomic fractions of the cations is rather small ($\sim 10^{-3}$), while it is much larger in the infinity norm ($\sim 10^{-1}$). In both norms, the error for the cations converges for a specific applied voltage difference ($\sim \delta\varphi = 5$). This can be explained because the Nernst-Planck model blocks the cation's share to go below zero. The error for the neutral solvent (green line) and the anions (blue line, on a large part below the green line) is increasing in both norms, for an increasing applied voltage difference and does seem to converge towards infinity.

5.5 Solvation Effect

As discussed in chapter 2, section 2.5, solvation leads to a clustering of a finite number of solvent molecules around an ion.

Figure 5.8: Influence of a on the pressure

Therefore, the specific Gibbs energy changes to

$$g_{\alpha} = g_{\alpha}^{\text{ref}} + (\kappa + 1) \frac{K}{m_{\alpha} n^{\text{ref}}} \ln \left(1 + \frac{p - p^{\text{ref}}}{K} \right) \quad (5.13)$$

$$g_N = g_N^{\text{ref}} + \frac{K}{m_{\alpha} n^{\text{ref}}} \ln \left(1 + \frac{p - p^{\text{ref}}}{K} \right) \quad (5.14)$$

The solvation effect is inspected on an incompressible, ternary electrolyte with the default values for λ^2 and a^2 and the following boundary conditions

$$\delta\varphi = 10.0 - 0.0 \quad (5.15)$$

$$p^R = 0.0 \quad (5.16)$$

$$y_{\alpha}^R = 0.01 \text{ for } \alpha \in \{A, C\} \quad (5.17)$$

Figure 5.11 visualizes the impact of the solvation number on the electric potential, pressure, anions-, cations-, and neutral solvent fractions. The different line styles indicate the different solvation numbers.

The electric potential's shape sharpens for an increased solvation number. The smaller the solvation number the smaller the range of the pressure values. Additionally, the pressure distribution gets more flat and has a wider solvation area for an increased solvation number.

The solvation number can also be identified as crucial for the height of the saturation level for the different species. For no solvation at all ($\kappa = 0$), the saturation level for the atomic fractions is at the values of zero and one. An increased solvation number, leading to an increased specific volume, leads to a smaller saturation height for the anions, but also to a wider solvation area in the electrolyte (compare with [5]). The solvation has a similar effect on the cations. The cations reach their saturation level earlier (coming from inside of the electrolyte), with an increased solvation number and have a wider solvation area. Contrary to this, the neutral solvent starts with a rather high fraction of 0.98, due to the choice of the anions and cations fraction inside the electrolyte. An increased solvation number leads to a wider solvation area for the neutral solvent and a higher saturation level, compared to a smaller solvation number (again, coming from inside the electrolyte).

Therefore, the solvation number can be identified to have a crucial impact on all the properties of interest. It changes the shape of the electric potential's distribution, the range of the pressure and the saturation level and solvation area of the ion fractions.

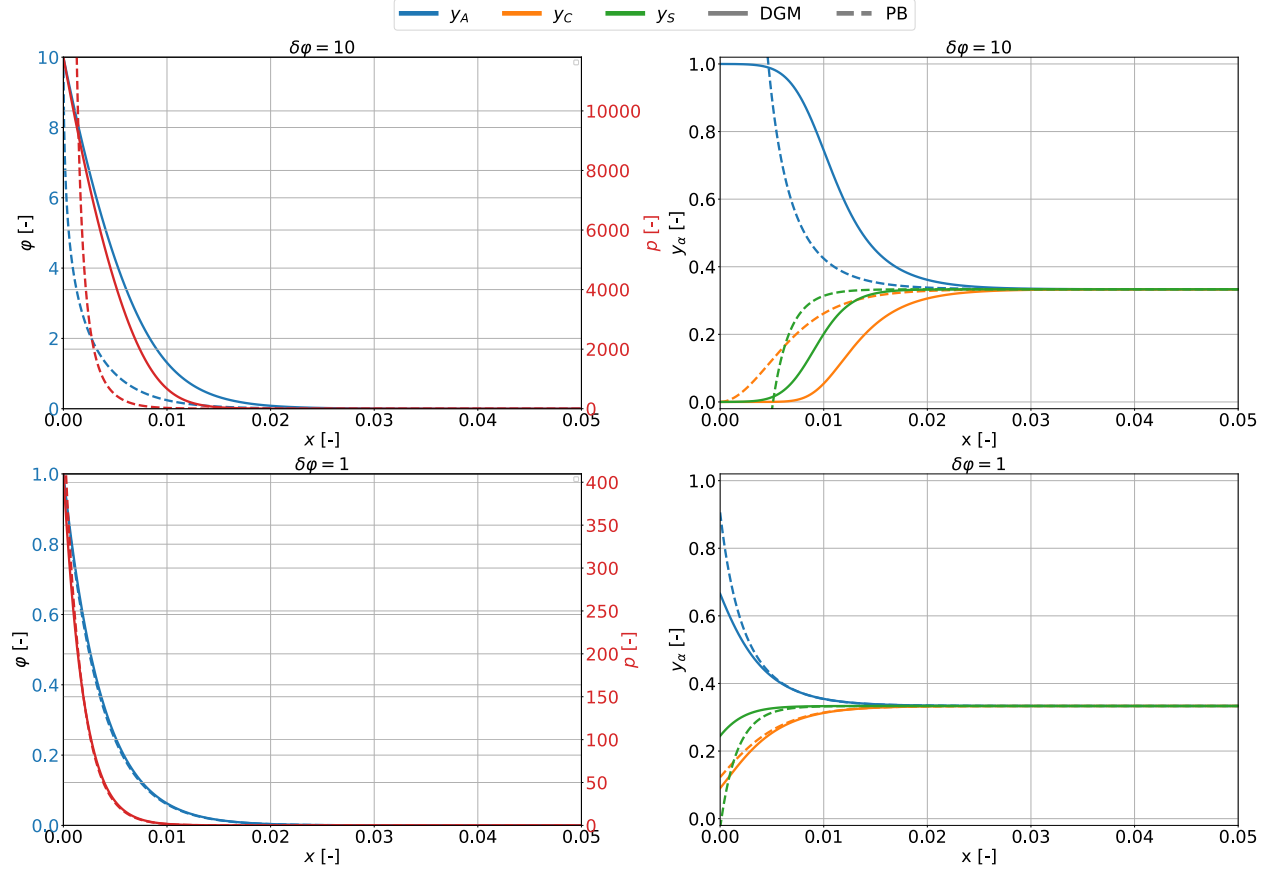


Figure 5.9: Comparison DGM model to Poisson-Boltzmann model

5.6 Compressibility

Yet, only incompressible mixtures were inspected. However, the influence of compressibility on the mixture can be of high interest. In this work, compressibility is represented by the value of K , representing the dimensionless bulk modulus multiplied by the reference pressure (recall $K \rightarrow p^{\text{ref}} K$). For incompressibility, let the bulk modulus go to infinity (compare with [3]). Therefore, the compressible mixture should converge towards an incompressible mixture, for increasing K .

The numerical results for the compressible electrolyte base on the boundary conditions

$$\delta\varphi = 6.0 \quad (5.18)$$

$$p^R = 0.0 \quad (5.19)$$

$$y_\alpha^R = \frac{1}{3} \text{ for } \alpha \in \{A, C\} \quad (5.20)$$

Refine for n_α

In Figure 5.12 the influence of the dimensionless bulk modulus on the electric potential (top left), cations- and anions distribution (top right), pressure (bottom left, logarithmic y-axis) and the total number of cations and anions (bottom right, logarithmic x-axis and logarithmic y-axis) can be seen. The different dimensionless bulk modulus are indicated by different colors. The blue line represents an incompressible solution, as a reference.

First of all, it can be identified that the solution converges towards the incompressible solution for an increasing K . For a value of $K = 15.000$ (orange line), the solution nearly covers the same line as the

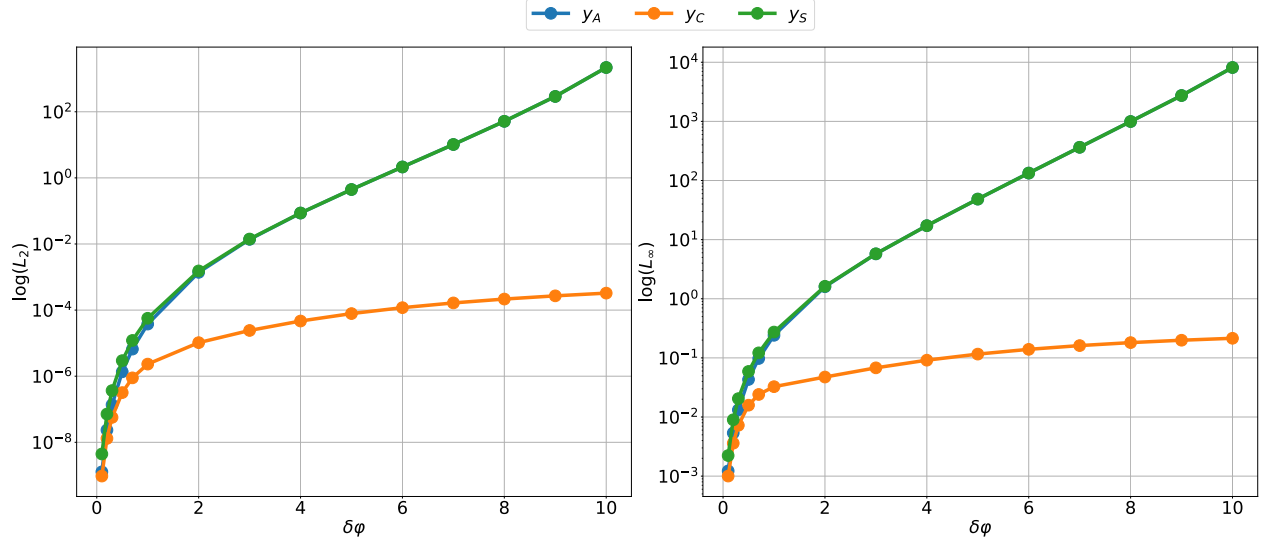


Figure 5.10: Convergence from DGM model towards Poisson-Boltzmann model

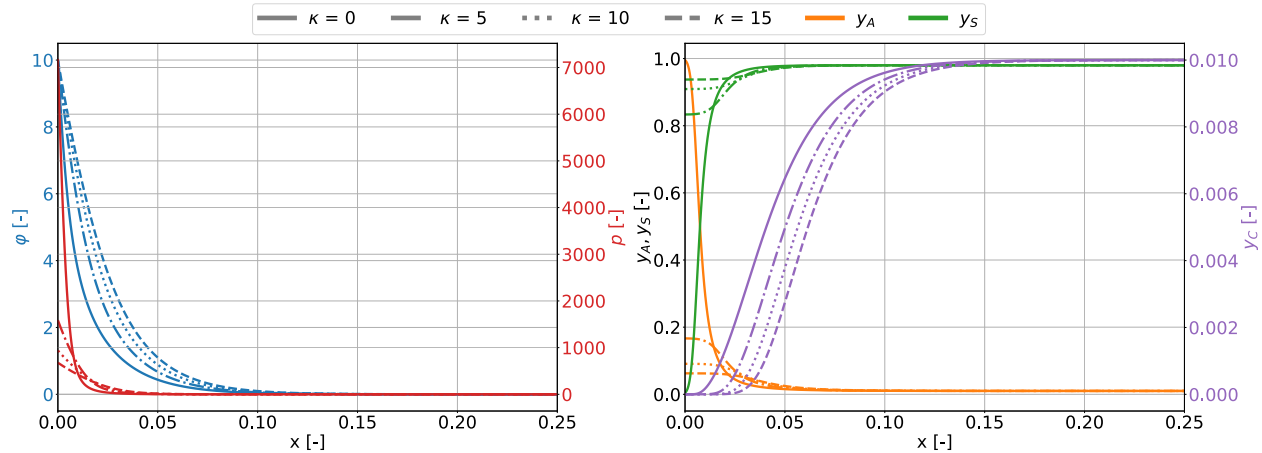


Figure 5.11: Effect of Solvation

incompressible solution (blue line). The lower the value for K , the more compressible the mixture and the larger the difference to the incompressible solution.

Increasing compressibility leads to a more bulbous shape for the electric potential. The fractional distribution of anions still reaches their saturation level at the value of one and the cations their at zero, not leaving the range of $[0, 1]$. Nevertheless, compressibility has an effect on the fractions, leading to a smaller part of the domain being covered fully by anions, for a more compressible mixture.

In an incompressible mixture the total number density is constant and therefore scaling the atomic fractions with this constant value yields the number densities. This is not the case for a compressible mixture, as the total number density is not constant anymore. In the presented case, the potential difference drives more particles to the left boundary, increasing the total number density on the left side. This leads to an exponentially increasing number of anions at the left side of the domain (see Figure 5.12 bottom right).

Similar to the total number density, the pressure is increasing for an increased compressibility, as the pressure is related to the total number density.

$$p = 1 + K(n - 1) \quad (5.21)$$

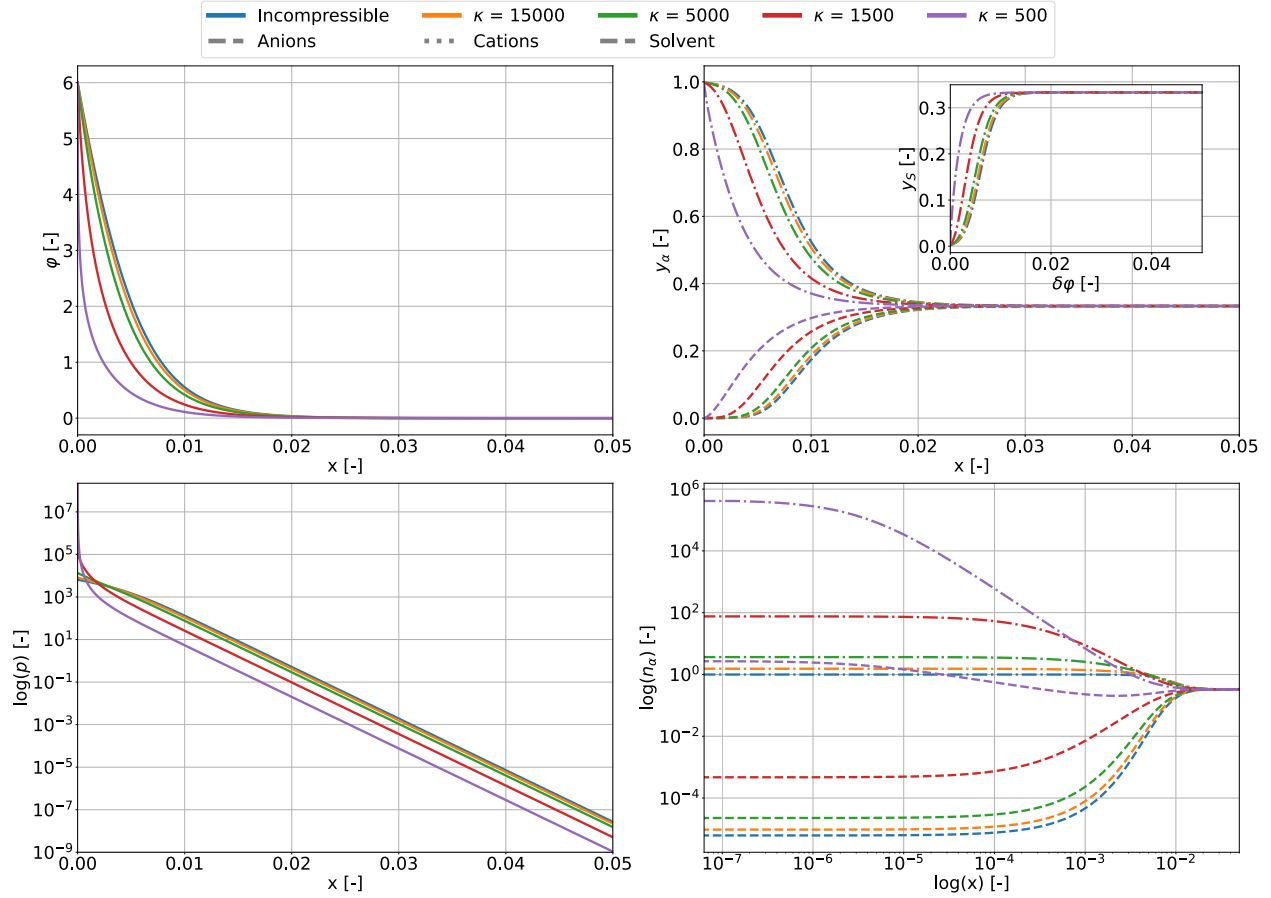


Figure 5.12: Compressibility

5.7 Double Layer Capacity

ToDo: Adapt labelsizes etc. for plots to be larger

The charge stored in the system is defined as the integral of the space charge, over the whole domain (see [9, 13]).

$$Q_{dl} = Q_{dl}(\varphi^L) = \int_{\Omega} n^F dx \quad (5.22)$$

The double layer capacity can then be calculated by the derivative of the charge with respect to the boundary value for the electric potential

$$C_{dl} = \frac{dQ_{dl}}{d\varphi^L} = \frac{d}{d\varphi^L} \int_{\Omega} n^F dx \quad (5.23)$$

In this section, the Dirichlet value for the atomic fractions on the right side of the domain depends on the molarity of the specific mixture

$$y_{\alpha}^R = \frac{M}{n^{\text{ref}}} \text{ for } \alpha \in \{A, C\} \quad (5.24)$$

with the molarity M and the reference number density n^{ref} . For the dimensionless parameters λ^2 and a^2 the default values are used.

All the solutions, presented in this section, are based on the reduced system of two equations, as discussed in chapter 3.

5.7.1 Influence of Molarity

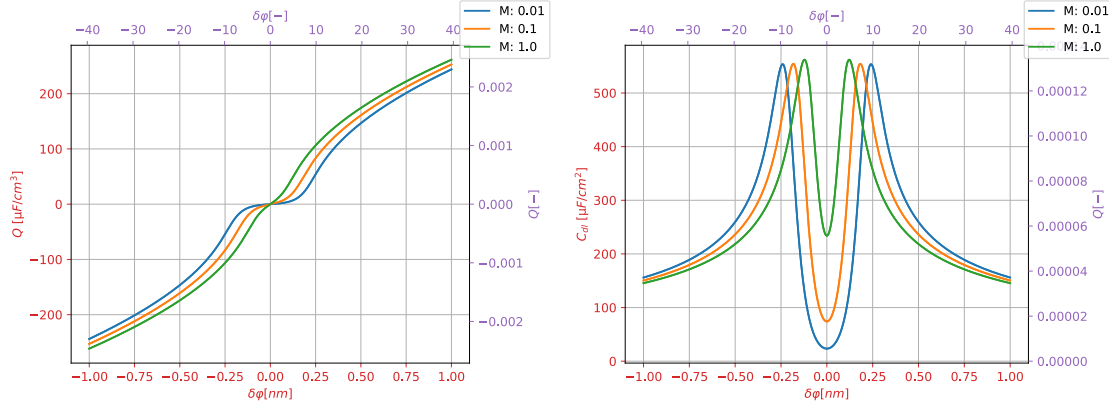


Figure 5.13: Calculation of the charge stored in the boundary and the double layer capacity for different molarities

The charge, stored in the system (top left), the double layer capacity (top right) and the value of the cations, anions and the neutral solvent at the leftmost point of the domain (bottom) are visualized in Figure 5.13. The y-axis shows the values for the property of interest, while the x-axis shows the applied potential difference.

No charge can be observed if there is no potential difference. This is expected since no potential difference leads to global charge neutrality and therefore to the space charge being zero over the whole domain.

Increasing the potential difference leads to an increased space charge. At a specific Voltage, the derivative of the charge increases and then decreases again. However, the space charge is strictly monotonously increasing. A larger molarity leads to a larger amount of cations and anions inside the electrolyte and to a larger charge, stored in the system.

The double layer capacity is larger than zero, even for no applied potential difference. However, the derivative for the capacity can be identified as zero, at this point. The capacity then starts to increase, till it reaches its maximum value and starts to decrease to an asymptotic value, outside of the domain. The molarity defines the height and the position of the local maxima. A higher molarity leads to a smaller local maximum, reached at a higher applied potential difference.

As the value of the molarity defines the value of the fractions for anions and cations inside the electrolyte, this value also defines the amount of both fractions at the left boundary. The anions and the neutral solvent reach their saturation point for a lower potential difference if the molarity is larger.

5.7.2 Influence of Dimensionless Parameter λ^2

As the parameter λ^2 has an influence on the distribution of the different atomic fractions, it is interesting to inspect the influence of this parameter on the double layer capacity. The double layer capacity highly depends on the space charge, which again depends on the atomic fractions. A larger value of λ^2 leads to a more bulbous shape for the fractions, indicating a larger charge and capacity.

Figure 5.14 proves this hypothesis. As assumed, the parameter λ^2 defines the height of the charge and the capacity. The larger the dimensionless parameter λ^2 the larger the charge, stored in the system, and the double layer capacity. This comes along with an increase of the temperature, the dielectric susceptibility or a decrease of the reference number density.

On the other hand, the value of the different ion fractions at the left side of the domain does not depend on the parameter λ^2 , as inspected in section 5.3. As the parameter a^2 was already proven to have no impact on the atomic fractions, this will also not change the space charge and therefore is of no interest in this analysis.

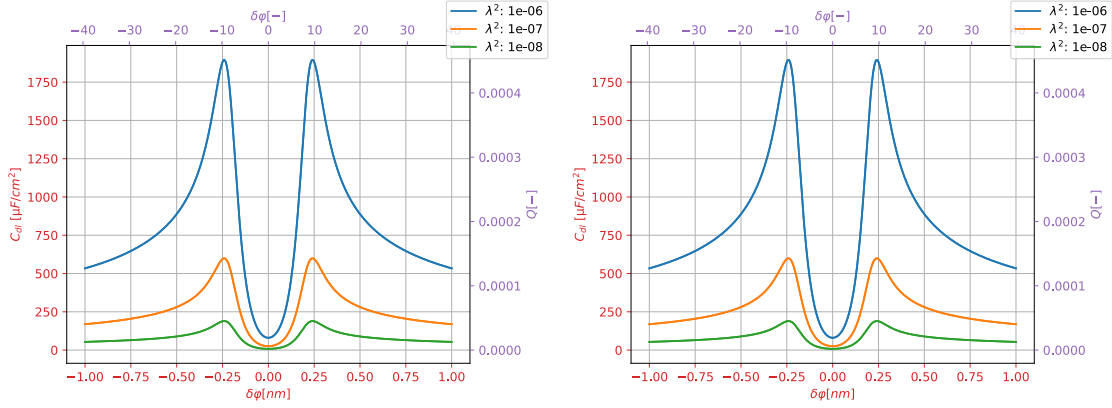


Figure 5.14: Calculation of the charge stored in the boundary and the double layer capacity for different values of λ^2

5.7.3 Influence of Compressibility

The space charge, in a compressible, ternary electrolyte, is calculated as

$$n^F = n(z_A y_A + z_C y_C) \quad (5.25)$$

As inspected in section 5.6 compressibility influences the number density and so the space charge, leading to a change of the charge of the system and the double layer capacity. The following calculations are performed on different scales of compressibility and a molarity of 0.01. The remaining parameters are chosen according to the values above.

Figure 5.15: Calculation of the charge stored in the boundary and the double layer capacity for different compressibilities

Figure 5.15 visualizes the influence of the dimensionless bulk modulus on the charge, stored in the system (top left), the double layer capacity (top right) and the number densities for the anions (bottom left), cations and the neutral solvent (bottom).

For an increasing bulk modulus, the solution converges towards the incompressible solution. Furthermore, a more compressible mixture leads to a larger charge. The double layer capacity reaches its highest value for a larger applied voltage and has a larger maximum value, the more compressible the mixture is. Additionally, for high compressibility, the course of the double layer capacity changes, compared to the incompressible case, as it reaches a local minimum after the local maximum and then rises asymptotically.

Furthermore, the number density of the anions at the left boundary increases for a larger bulk modulus, for an applied potential difference larger than a certain value (~ 10). The influence of the compressibility on the number density of cations and the neutral solvent at the left boundary is neglectable.

5.8 Many Constituent Mixture

For now, a mixture of three constituents was analyzed. Nevertheless, it can be interesting to study the influence of many different constituents on the electrolyte. In this case, the space charge n^F is calculated as

$$n^F = \sum_{\alpha=1}^{N-1} (z_{\alpha} y_{\alpha}) \quad (5.26)$$

with $N \neq 3$. Each extra constituent adds an extra partial mass balance to the system, that needs to be solved, ending with $N + 1$ partial differential equations.

In the following, a mixture with four, five and six different constituents, each with a neutral solvent, will be presented on the one dimensional domain $\Omega = [0, 1]$.

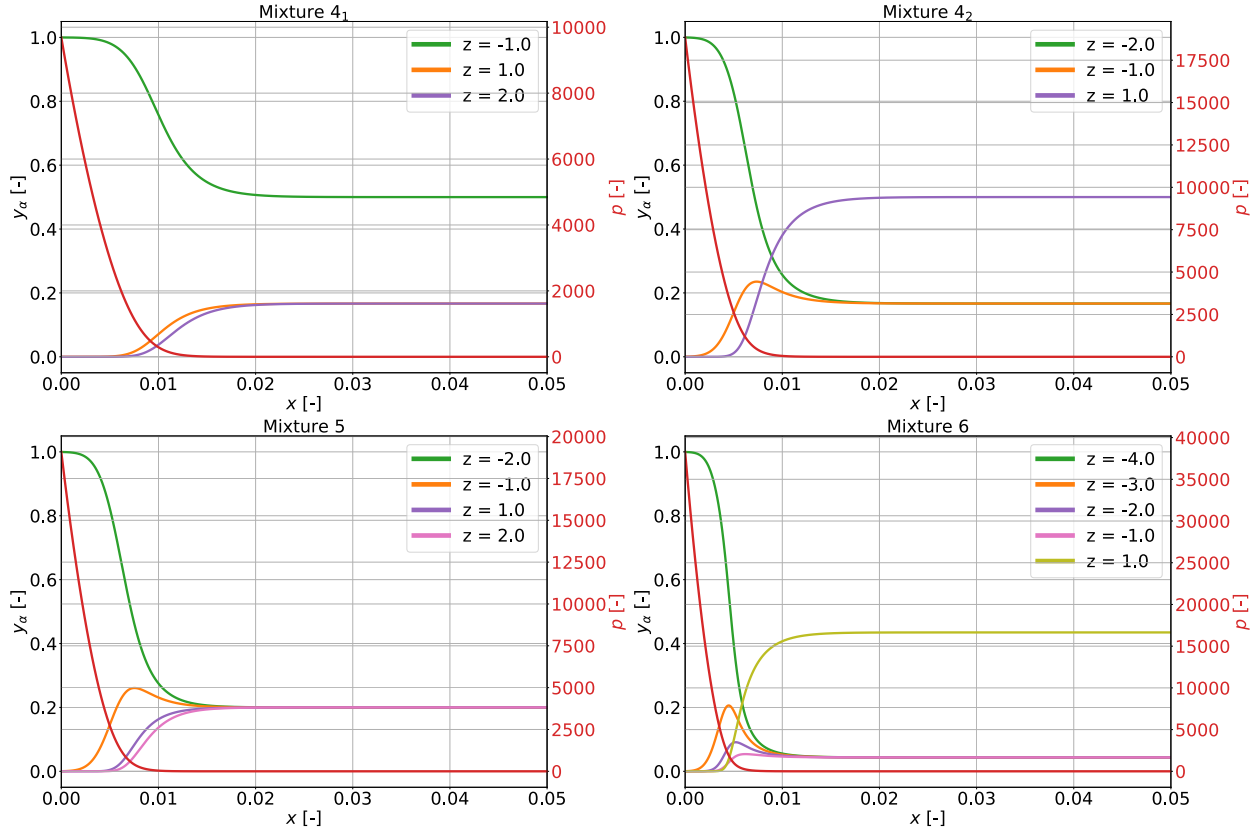


Figure 5.16: Atomic fractions (left axis) and pressure (right axis) for all four different mixtures

5.8.1 Four Constituents

First, a mixture with four different constituents will be inspected. Two solutions are presented, one with two species with positively charged anions and one species with negatively charged ones (mixture $\cdot^{(1)}$), and vice versa (mixture $\cdot^{(2)}$). All mixtures are assumed to be incompressible and in equilibrium. Furthermore, the potential difference was set to 10.0, with a vanishing pressure at the right side of the domain. The charge numbers are set to

$$z_1^{(1)} = -1.0, \quad z_2^{(1)} = 1.0, \quad z_3^{(1)} = 2.0 \quad (5.27)$$

$$z_1^{(2)} = -2.0, \quad z_2^{(2)} = -1.0, \quad z_3^{(2)} = 1.0 \quad (5.28)$$

and the atomic fractions at the right boundary are

$$y_1^{R,(1)} = \frac{3}{6}, \quad y_2^{R,(1)} = \frac{1}{6}, \quad y_3^{R,(1)} = \frac{1}{6} \quad (5.29)$$

$$y_1^{R,(2)} = \frac{1}{6}, \quad y_2^{R,(2)} = \frac{1}{6}, \quad y_3^{R,(2)} = \frac{3}{6} \quad (5.30)$$

to initialize local charge neutrality in the inner of the electrolyte.

In Figure ?? mixture one $(z^{(1)}, y^{(1)})$ and in Figure ?? mixture two $(z^{(2)}, y^{(2)})$ is presented. As in section 5.2 observed, the negative charged ion's share increases towards the boundary, while the share of positively

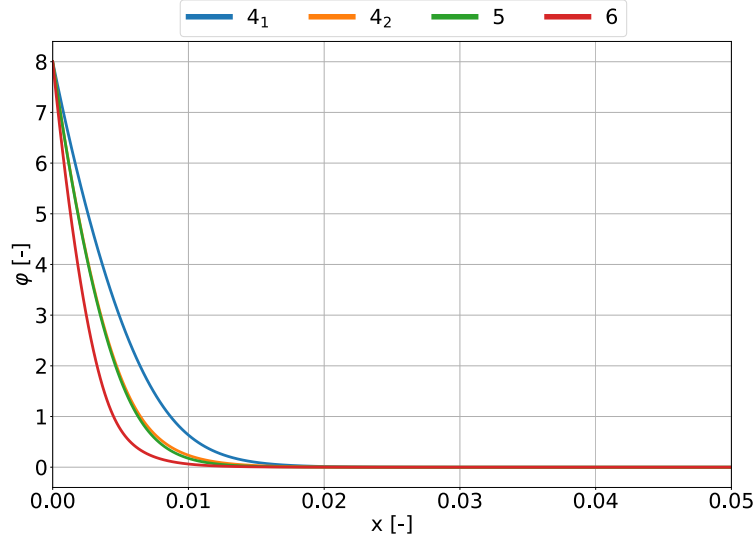


Figure 5.17: Electric Potential for all four different mixtures

charged anions decreases. For mixture one, the negatively charged anions grow, till they reach the upper saturation level of one, while the positively charged cations and the neutral solvents fraction decreases towards zero. The higher the charge number, the faster the constituent's fractions go to zero.

For mixture two all positively charged ions and the neutral solvents fraction tend to go towards zero at the left boundary. However, in this case, not all negatively charged constituents go towards the upper saturation level of one. The less negatively charged constituents fraction ($z = -1$) first increases towards a local maximum but then decreases towards zero. The more negatively charged constituents fraction ($z = -2$) increases towards the upper saturation level of one, as before. However, the part of the domain, which is fully covered with this constituent is smaller, compared to mixture one.

The pressure, however, seems to be scaled roughly by a factor of two for mixture two, compared to mixture one, indicating that the largest negative charge number decides this scaling. Mixture one has a maximum pressure of 7.306 dimensionless units, while mixture two has a maximum pressure of 14.208 dimensionless units. This will be further inspected in subsections 5.8.2 and 5.8.3. An analysis for the electric potential will be done in section 5.8.4, and therefore be skipped in this section and the following sections.

5.8.2 Five Constituents

Next, a single mixture with five different constituents

$$z_1 = -2.0, \quad z_2 = -1.0, \quad z_3 = 1.0, \quad z_4 = 2.0, \quad z_5 = z_N = 0 \quad (5.31)$$

will be inspected. Inside the electrolyte, the fractions are evenly distributed

$$y_\alpha = \frac{1}{5} \quad \alpha = \{1, \dots, 5\} \quad (5.32)$$

leading to local charge neutrality at the right boundary.

Figure ?? shows these five different constituents. Again, the atomic fraction of the species with the smallest charge number ($z = -2$) goes towards the upper saturation level at the left boundary. The other, negatively charged constituent's ($z = -1$) atomic fraction rises towards a local maximum before it falls to the lower boundary of zero. The positively charged species and the neutral solvents share decreases towards zero, with a steeper decrease, the larger the charge number is.

In this mixture, the maximum pressure value is 14.390 dimensionless units, again in the same size as mixture two in section 5.8.1 for the identical smallest charge number.

5.8.3 Six Constituents

Lastly, a mixture with six different constituents will be inspected.

$$z_1 = -4.0, \quad z_2 = -3.0, \quad z_3 = -2.0, \quad z_4 = -1.0, \quad z_5 = 1.0, \quad z_6 = z_N = 0.0 \quad (5.33)$$

Again, the mixture is initialized with local charge neutrality inside the electrolyte, leading to

$$y_1^R = y_2^R = y_3^R = y_4^R = \frac{1}{23}, \quad y_5^R = \frac{10}{23} \quad (5.34)$$

The fraction of the constituent with the smallest charge number goes towards the upper saturation level of one. The fraction of the other negatively charged constituents rises towards a local maximum and then decreases towards the lower boundary value of zero. Additionally, the size of the local maximum is larger, the smaller the charge number is. The positively charged constituents and the neutral solvents share go towards the lower saturation level of one. The positively charged constituent reaches this lower level faster, compared to the neutral solvent.

The maximum pressure is 28.863 dimensionless units with the smallest charge number $z_1 = -4.0$. Therefore, the assumption, that the smallest charge number scales the pressure can be verified for the four different tested mixtures.

5.8.4 Electric Potential in a Many Constituent Mixture

For now, only the pressure and the atomic fractions for the different mixtures of different numbers of species were compared. In the above visualizations, a difference in the electric potential between the different mixtures can hardly be seen, Figure ?? presents all the different electric potentials in a single figure.

Index 4₁ presents the electric potential for mixture one, consisting of four different species, from section 5.8.1, 4₂ mixture two from the same section, index 5 presents the mixture from section 5.8.2 and index 6 the mixture consisting of six different constituents, presented in Figure 5.8.3. There is a difference in the electric potential between the four different mixtures. Mixture 4₁ has the most bulbous shape, while mixture 6 has the sharpest shape. The electric potential for mixtures 4₂ and mixture 5 is somewhere between those two. The smallest charge number for mixtures 4₂ and 5 are both -2 , while the smallest charge number for mixture 4₁ is -1 and for mixture 6 it is -4 . This indicates that the smallest charge number decides the shape of the electric potential. However, there is a slight difference between mixtures 4₂ and 5. The electric potential of mixture 5 has a sharper shape, compared to mixture 4₂. The sum over all charge numbers for mixture 5 is 0, while the sum over all charge numbers for mixture 4₂ is -1 . This indicates that the sum of all charge numbers also impacts the solution of the electric potential.

5.9 2D-Results

5.9.1 Electric Diode

`solver.convergence_criterion = 'residual' -> converges to $\text{rtol}=1\text{e-}8$, but "incremental" gets stuck at $\text{rtol}=1\text{e-}5$ -> indicates numerical instability???`

Rectification cannot be observed, maybe because Fuhrmann used specific volume different for solvent and anions, cations? He also didnt take pressure into account, shouldnt be that much of a problem

In the next example, a two dimensional electrolytic diode is analyzed. Two baths, with a certain anion and cation concentration, are connected by a nanofluidic channel. On one side of the channel, pore charges are applied as Neumann boundary conditions (see [14])

Regard a ternary electrolyte in the two dimensional domain $\Omega = [0, 2] \times [0, 10]$ with the dimensionless parameter $\lambda^2 = 1 \cdot 10^{-7}$ and $a^2 = 1 \cdot 10^{-4}$. The bath concentrations are $y_A^{\text{bath}} = y_C^{\text{bath}} = 0.04$ at $(x, y) = (x, 0)$ and $(x, y) = (x, 10)$. At $(x, y) = (x, 0)$ the electric potential is $\varphi = 0$, while at $(x, y) = (x, 10)$ a bias in the electric potential φ_{bias} is applied. The following Neumann boundary condition is applied for the electric potential

$$\nabla\varphi \cdot \vec{n} = g_\varphi = \begin{cases} \sigma & , (x = 2, \frac{1}{2} \leq y \leq \frac{3}{4}y) \\ -\sigma & , (x = 2, \frac{1}{4} \leq y < \frac{1}{2}y) \\ 0 & , \text{else} \end{cases} \quad (5.35)$$

with $\sigma = 5$ (compare with [10]).

Figure ?? shows the results when applying a forward bias ($\varphi_{\text{bias}} = 10.0$), Figure ?? shows the results for no bias ($\varphi_{\text{bias}} = 0.0$) and Figure ?? a backward bias ($\varphi_{\text{bias}} = -10.0$) is applied. The line, along the channel center, of all five properties is visualized in Figure ?. One more time, it can be verified that neither of the atomic fractions goes beyond the saturation level of zero and one. However, in this case, both the anions fractions and cations fractions nearly cover the full range of possible values over the complete domain. For all different applied biases, the share of negatively charged anions reaches its maximum in the center of the negative Neumann boundary conditions ($x = 2, y = 0.375$), while the positively charged cations reach their maximum value in the center of the positive Neumann boundary condition ($x = 2, y = 0.635$). For both species, the atomic fraction gets very close to the upper boundary value of one. Following this and the definition for $y_S = y_N = 1 - \sum_{\alpha=1}^{N-1} y_\alpha$, the neutral solvents share has its minimum close to zero, at these points. For the electric potential and the pressure, there is a larger difference between the three different examples. However, in all three scenarios, the electric potential has a maximum in the center of the negative Neumann boundary condition and a minimum in the center of the positive Neumann boundary condition, while the pressure has a maximum in both points.

For the forward bias (see Figure ??), the electric potential rises from its minimum at the bottom boundary ($\varphi|_{(x,y)=(x,0)}$) to the global maximum at the upper boundary ($\varphi|_{(x,y)=(x,10)} = \varphi_{\text{bias}}$). On its way, it passes a local maximum and a local minimum, due to the two Neumann boundary conditions. The electric potential from the two local maxima diffuses almost horizontally, while the pressure is pressed between the two maxima at the Neumann boundary conditions, resulting in a comparably low pressure at the upper and lower boundary.

With no applied bias (see Figure ??), the electric potential reaches its global extrema at the points of the center of the Neumann boundary conditions. These maximum and minimum diffuse away from the points, with a slight shift to the outside of the domain. The pressure, on the other hand, is neither pressed between the two maxima nor away from these. The pressure has a local minimum in the middle of the domain and on the bottom and the top of it. The maxima from the Neumann boundary condition diffuse marginally to the bottom and top sides of the domain.

For a backward bias (see Figure ??), the electric potential first increases, coming from the bottom boundary to a certain point, then rapidly decreases, and then starts to increase again. The pressure begins to increase exponentially for increasing y , till it reaches its global maximum, then rapidly decreases towards the global minimum before rapidly increasing to a local maximum, again. After this, it falls again towards a constant value on the top boundary.

Non symmetry:

- Too coarse discretization?
- Other reasons?

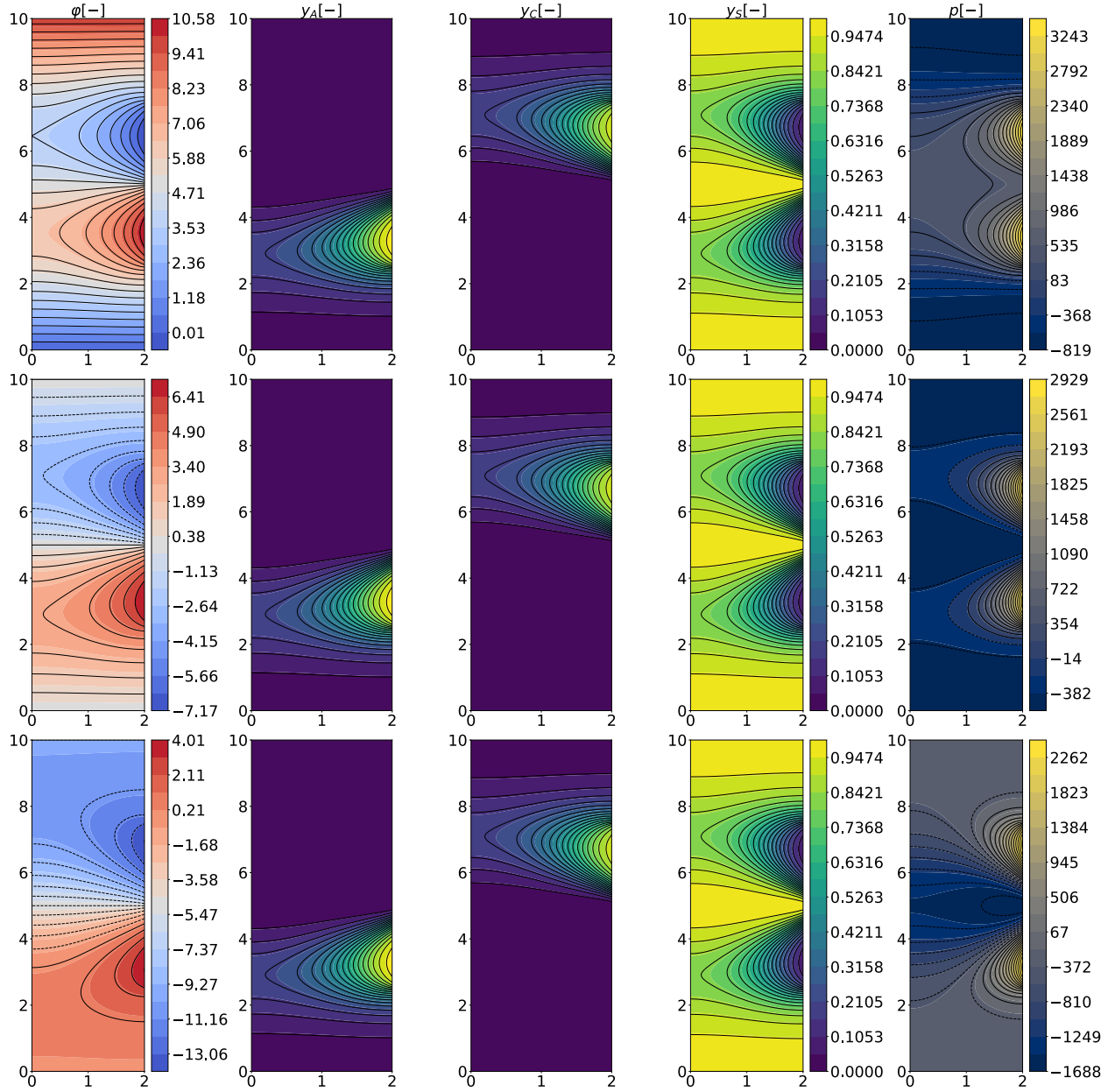


Figure 5.18: Forward Bias (top, $\varphi_{\text{bias}} = 10$), no bias (center, $\varphi_{\text{bias}} = 0$) and backward bias (bottom, $\varphi_{\text{bias}} = -10$)

Bibliography

- [1] Stefanie Braun, Chihiro Yada, and Arnulf Latz. Thermodynamically consistent model for space-charge-layer formation in a solid electrolyte. *The Journal of Physical Chemistry C*, 119(39):22281–22288, 2015.
- [2] W. Dreyer, C. Gohlke, and M. Landstorfer. A mixture theory of electrolytes containing solvation effects. *Electrochemistry Communications*, 43:75–78, 2014.
- [3] Wolfgang Dreyer, Clemens Gohlke, and Rüdiger Müller. Overcoming the shortcomings of the nernst-planck model. *Phys. Chem. Chem. Phys.*, 15:7075–7086, 2013.
- [4] Wolfgang Dreyer, Clemens Gohlke, and Rüdiger Müller. Modeling of electrochemical double layers in thermodynamic non-equilibrium. *Phys. Chem. Chem. Phys.*, 17:27176–27194, 2015.
- [5] Wolfgang Dreyer, Clemens Gohlke, and Rüdiger Müller. Bulk-surface electrothermodynamics and applications to electrochemistry. *Entropy*, 20(12), 2018.
- [6] J. Fuhrmann. A numerical strategy for nernst-planck systems with solvation effect. *Fuel Cells*, 16(6):704–714, 2016.
- [7] Jürgen Fuhrmann. LiquidElectrolytes.jl, August 2024.
- [8] Jürgen Fuhrmann, Clemens Gohlke, Alexander Linke, Christian Merdon, and Rüdiger Müller. Models and numerical methods for electrolyte flows. In Michael Hintermüller and José Francisco Rodrigues, editors, *Topics in Applied Analysis and Optimisation*, pages 183–209, Cham, 2019. Springer International Publishing.
- [9] Jürgen Fuhrmann. Comparison and numerical treatment of generalised nernst-planck models. *Computer Physics Communications*, 196:166–178, 2015.
- [10] Benoît Gaudeul and Jürgen Fuhrmann. Entropy and convergence analysis for two finite volume schemes for a Nernst-Planck-Poisson system with ion volume constraints. *Numerische Mathematik*, 151(1):99–149, April 2022.
- [11] Jan Habscheid. Reproducibility Repository for: Numerical Treatment of a Thermodynamically Consistent Electrolyte Model (B.Sc. Thesis - Jan Habscheid), September 2024.
- [12] Sebastian Krumschein. Numerical methods for partial differential equations - lecture notes for ces and sisc. 2021.
- [13] M. Landstorfer, C. Gohlke, and W. Dreyer. Theory and structure of the metal-electrolyte interface incorporating adsorption and solvation effects. *Electrochimica Acta*, 201:187–219, 2016.
- [14] Bartłomiej Matejczyk, Mónika Valiskó, Marie-Therese Wolfram, Jan-Frederik Pietschmann, and Dezső Boda. Multiscale modeling of a rectifying bipolar nanopore: Comparing poisson-nernst-planck to monte carlo. *The Journal of Chemical Physics*, 146(12), March 2017.
- [15] Walther Nernst. Die elektromotorische wirksamkeit der jonen. *Zeitschrift für Physikalische Chemie*, 4U(1):129–181, 1889.

- [16] Max Planck. Ueber die erregung von electricität und wärme in electrolyten. *Annalen der Physik*, 275(2):161–186, 1890.
- [17] Max Planck. Ueber die potentialdifferenz zwischen zwei verdünnten lösungen binärer electrolyte. *Annalen der Physik*, 276(8):561–576, 1890.
- [18] Prohl, Andreas and Schmuck, Markus. Convergent finite element discretizations of the navier-stokes-nernst-planck-poisson system. *ESAIM: M2AN*, 44(3):531–571, 2010.
- [19] Tomáš Roubíček. Incompressible ionized fluid mixtures. *Continuum Mechanics and Thermodynamics*, 17(7):493–509, May 2006.

Appendix A: Detailed Proof of the Incompressible Limit

$$\lim_{K \rightarrow \infty} g_\alpha = \lim_{K \rightarrow \infty} \left(g_\alpha^{\text{ref}} + (\kappa + 1) \frac{K}{m_\alpha n^{\text{ref}}} \ln \left(1 + \frac{p - p^{\text{ref}}}{K} \right) \right) \quad (36)$$

$$= g_\alpha^{\text{ref}} + (\kappa + 1) \frac{1}{m_\alpha n^{\text{ref}}} \lim_{K \rightarrow \infty} \left(K \ln \left(1 + \frac{p - p^{\text{ref}}}{K} \right) \right) \quad (37)$$

$$= g_\alpha^{\text{ref}} + (\kappa + 1) \frac{1}{m_\alpha n^{\text{ref}}} \lim_{K \rightarrow \infty} \lim_{K \rightarrow \infty} \left(\frac{\ln(1 + \frac{p - p^{\text{ref}}}{K})}{\frac{1}{K}} \right) \quad (38)$$

$$= g_\alpha^{\text{ref}} + (\kappa + 1) \frac{1}{m_\alpha n^{\text{ref}}} \lim_{K \rightarrow \infty} \underbrace{\left(\frac{\frac{1}{1 + \frac{p - p^{\text{ref}}}{K}} - \frac{(p - p^{\text{ref}})}{K^2}}{\frac{-1}{K^2}} \right)}_{\text{l'Hospital}} \quad (39)$$

$$= g_\alpha^{\text{ref}} + (\kappa + 1) \frac{1}{m_\alpha n^{\text{ref}}} \lim_{K \rightarrow \infty} \left(\frac{1}{1 + \frac{p - p^{\text{ref}}}{K}} \frac{p - p^{\text{ref}}}{K^2} K^2 \right) \quad (40)$$

$$= g_\alpha^{\text{ref}} + (\kappa + 1) \frac{1}{m_\alpha n^{\text{ref}}} (p - p^{\text{ref}}) \quad (41)$$

Appendix B: Derivation of the Variational Formulation

Derivation of the variational formulation.

Recall Gauss integration theorem in the many-dimensional case

$$\int_{\Omega} y \operatorname{div}(\vec{v}) dV = \int_{\partial\Omega} y \vec{v} \cdot d\vec{S} - \int_{\Omega} \vec{v} \cdot \operatorname{grad}(y) dV \quad (42)$$

For the variational formulation, the divergence of 2.45 is taken.

$$\begin{aligned} 0 &= \int_{\Omega} \begin{bmatrix} \lambda^2 \Delta \varphi + n^F \\ \operatorname{div}(a^2 \nabla p + n^F \nabla \varphi) \\ \operatorname{div}(\mathbf{J}_1) \\ \vdots \\ \operatorname{div}(\mathbf{J}_{N-1}) \end{bmatrix} \cdot \begin{bmatrix} v_{\varphi} \\ v_p \\ v_{y_1} \\ \vdots \\ v_{y_{N-1}} \end{bmatrix} d\Omega \\ &= \int \left(\underbrace{(\lambda^2 \Delta \varphi + n^F) \cdot v_{\varphi}}_{B1} + \underbrace{\operatorname{div}(a^2 \nabla p + n^F \nabla \varphi) \cdot v_p}_{B2} + \sum_{\alpha=1}^{N-1} \underbrace{\operatorname{div}(\mathbf{J}_{\alpha}) \cdot v_{y_{\alpha}}}_{B3} \right) \end{aligned} \quad (43)$$

Next, Gauss theorem is applied on $B1, B2$ and $B3$.

For $B1$.

$$\begin{aligned} &\int_{\Omega} (\lambda^2 \Delta \varphi + n^F) \cdot v_{\varphi} d\Omega = 0 \\ &\Leftrightarrow \int_{\Omega} \lambda^2 \Delta \varphi \cdot v_{\varphi} d\Omega - \int_{\Omega} n^F \cdot v_{\varphi} d\Omega = 0 \\ &\int_{\Omega} \lambda^2 \nabla \varphi \cdot \nabla v_{\varphi} d\Omega - \int_{\Gamma_N} \lambda^2 \nabla \varphi \cdot \vec{n} v_{\varphi} ds - \int_{\Omega} n^F \cdot v_{\varphi} d\Omega = 0 \end{aligned}$$

Next, for $B2$.

$$\int_{\Omega} \operatorname{div}(a^2 \nabla p + n^F \nabla \varphi) \cdot v_p d\Omega = 0 \quad (44)$$

$$\int_{\Omega} (a^2 \nabla p + n^F \nabla \varphi) \cdot \nabla v_p d\Omega - \int_{\Gamma_N} (a^2 \nabla p + n^F \nabla \varphi) \cdot \vec{n} v_p ds = 0 \quad (45)$$

Last, for $B3$.

$$\int_{\Omega} \operatorname{div}(\mathbf{J}_{\alpha}) \cdot v_{y_{\alpha}} d\Omega = 0 \quad (46)$$

$$\int_{\Omega} \mathbf{J}_{\alpha} \cdot \nabla v_{y_{\alpha}} d\Omega - \int_{\Gamma_N} \mathbf{J}_{\alpha} \cdot \vec{n} v_{y_{\alpha}} = 0 \quad (47)$$

Lastly, $B1, B2$ and $B3$ are inserted back into (43) and the proposed variational formulation can be observed.

$$\int_{\Omega} \nabla \varphi \cdot \nabla v_{\varphi} d\Omega - \int_{\Gamma_N} g_{\varphi} v_{\varphi} ds - \int_{\Omega} \frac{1}{\lambda^2} n^F d\Omega \quad (48)$$

$$+ \int_{\Omega} \left(\nabla p + \frac{1}{a^2} n^F \nabla \varphi \right) \cdot \nabla v_p d\Omega - \int_{\Gamma_N} g_p v_p ds \quad (49)$$

$$+ \sum_{\alpha=1}^{N-1} \left(\int \mathbf{J}_{\alpha} \cdot \nabla v_{y_{\alpha}} - \int_{\Gamma_N} g_{y_{\alpha}} v_{y_{\alpha}} ds \right) \quad (50)$$

$$=0 \quad (51)$$